Fall 2010

Controlling strength and permeability of silica investment casting molds

Darryl M. Kline

CONTROLLING STRENGTH AND PERMEABILITY OF SILICA INVESTMENT CASTING MOLDS

by

DARRYL MICHAEL KLINE

A THESIS

Presented to the Faculty of the Graduate School of the

MISSOURI UNIVERSITY OF SCIENCE AND TECHNOLOGY

In Partial Fulfillment of the Requirements for the Degree

MASTER OF SCIENCE IN METALLURGICAL ENGINEERING

2010

Approved by

Von L. Richards, Advisor
Kent Peaslee
Jeffrey Smith

ABSTRACT

Investment casting is a metal casting process in which a ceramic mold is created around a disposable pattern using dip coating. The fine silica flour making up most of the mold gives the benefits of a smooth internal mold surface and high density. The high density allows for investment casting molds to be thinner and lighter than sand-based molds, but gives substantially smaller gaps between particles for air flow.

This research focused on the design and improvement of the formulation for making investment casting molds with customizable physical properties. Properties of the molds, specifically flexural strength, permeability, and physical structure, were monitored and used as references for optimizing the formulation. Experiments were performed for this research to determine preferred parameters: size range of the stucco particles, the ceramic slurry viscosity, and whether sacrificial particles should be added to the slurry to increase pore volume and in what concentrations.

It was determined that thicker molds displayed higher strength, but slower air expulsion rates through them when compared to thinner molds. Factors that increased mold thickness included applying larger diameter stucco particles, using more viscous ceramic slurry that gives a higher coating thickness, and applying additional coating layers. Factors to increase volumetric air flow through the mold include applying fewer coating layers, using less viscous slurry to change from a layered to a monolithic mold structure and decrease apparent density, and increasing the size and concentration of pores within the mold.

ACKNOWLEDGEMENTS

I would like to thank Dr. Von Richards and Dr. Simon Lekakh for their assistance with determining the direction of this research and their feedback concerning data analysis. Much thanks also goes to U.S. Army Benet Laboratories for their funding of my research.

Other people of note are Dr. Kent Peaslee and Dr. Jeffrey Smith for their help reviewing this thesis. Assistance by fellow graduate research assistants during casting trials was greatly appreciated. Of the other research students I would like to specifically acknowledge Chirag Mahimkar, Abhilash Dash, and Maj. Ryan Howell for there assistance in compiling material data I used for casting simulations.

A special thank you goes to my parents Philip and Colleen Kline for there continued support and encouragement through the years. I also appreciate my grandparents for keeping me in their thoughts and prayers. Thanks also to my brother, Dexter, my friends up in Michigan, and the underclassmen back at Rose-Hulman for giving me something to look forward to whenever I could escape for a vacation.

TABLE OF CONTENTS

Page

LIST OF ILLUSTRATIONS

LIST OF TABLES

1. INTRODUCTION

1.1. BACKGROUND

The investment casting process has been around for centuries, though originally referred to as the lost wax process. Evidence of its use has been noted for both small jewelry and large statues by archeologists all over the world. Originally only metals with low melting points like bronze and gold were used because of melting technology. The process was re-discovered in the modern era by B. F. Philbook in 1897 for production of dental fillings and inlays. Foundries started to use the process during World War II as a method to limit welding and machining requirements.[1]

The main advantage investment casting has over other casting methods is that it allows the casting of a near net-shape product. This is made possible by the use of wax (or foam) as a removable mold pattern. The lower strength and melting point of wax makes it easier to sculpt to the desired dimensions than to alter a block of metal.

The mold used for investment casting is created by dipping the pattern into ceramic slurry containing very fine ceramic flour and a ceramic based binder. The liquid slurry covers the pattern where it is allowed to dry and gel together. Upon each dip coating a layer of large grain ceramic stucco is sprinkled. This dipping process is continued until the mold will have enough strength to withstand the stresses exerted on it during pattern removal and metal casting.

There are four different type of coating layers that are used to make investment casting molds: prime, intermediate, backup, and seal. Prime coats are the first layer and commonly uses the highest slurry viscosity of the coatings since it is applied to a smooth

pattern surface that limits adherence. The prime slurry also tends to use different materials since the use of zircon is advantageous because of its higher thermal conductivity. Fine grained stucco is used for the prime coat to prevent it from penetrating through the layer and affecting the mold's internal surface quality. Some foundries use a second prime coat to cover any spots missed by the first prime coat and to create a thicker region of the mold containing zircon.

An intermediate coat between the prime and backup layers is not used by all foundries. Those that apply one use the backup slurry with stucco whose grain size is between that used for the prime and backup coats. It is believed by some that using the intermediate stucco limits the size of inter-stucco voids near the metal-mold interface and preventing deep metal penetration if a mold crack is formed.[2]

The backup coatings are primarily where the strength of the mold lies. The presence of inter-stucco voids and stucco penetration through layers are not as much a concern as in previous layers. Quite the opposite tends to be true in the backup layers. Voids within the interior of the mold tend to aid in gas and wax removal during mold construction and casting. Since the presence of voids helps gas, water, and melted wax flow, and thicker molds have more strength, it is common to use relatively large grained stucco for the backup layers which increase mold thickness and have a looser packing.

The final coating layer is the seal coat. The slurry is the same as for the backup, but without stucco being applied. This coating helps to prevent abrasive removal of stucco from the final backup coat during handling. The removal of stucco from the mold can contaminate the surrounding environment as well as introduce cracks.

1.2. LITERATURE REVIEW

The process for investment casting has many different forms, all of which have been proven through use in different foundries. The materials used for the mold vary among silica, zircon, alumina, other proprietary ceramics, and blends of each. The current dominant choice for a binder is colloidal silica, ever since the United States government imposed limits on the use of ethyl silicate.

The size and shape of the solids in the colloidal silica varies among the manufacturers as does their selection of proprietary additives like anti-foaming agents, wetting agents, and sodium concentrations. The weight ratio between the flour and binder, as well as dilution of the binder varies greatly among foundries. A small number of researchers have attempted to determine optimal ratios for materials, but they require an intimate knowledge of the flour and binder particles' shapes, size distribution, and acidity as well as the complete composition of the binder.[3,4]

The operating viscosity of the slurries is different for each foundry, as well as the allowable range from that target viscosity. It is common that the viscosity of the prime slurry is higher than the backup slurry, but the difference changes based on materials used and what each individual foundry finds to work for their own operation.

The selection of stucco also differs between foundries. The use of fused silica and alumino-silcate tend to be the top choices, but the particle size distribution is not standard for all.

As presented above, the investment casting process is not just a science, but also an art in which a wide selection of materials and parameters may be chosen to match individual needs and preferences. The research findings presented in the remainder of

this section will try to remain generalized so to be useful to all processes. Because the focus of the research presented in this thesis deals primarily with mold permeability and strength, the discussion of thermal properties, other than during mold firing, will not be included.

1.2.1. Mold Processing. Each of the four types of coatings applied to an investment casting mold use differing slurry parameters and stucco, so it should stand to reason that each affects the physical properties of the mold in a different way. Higher viscosity for the prime slurry gives a different coating thickness than the lower viscosity backup slurry. The different particle sizes of the stucco when matched with coating thicknesses can lead to different layer structures in the mold.

1.2.1.1. Layer differences. Work recently done by C. Whitehouse and B. Dahlin concerning autoclave cracking had them comparing the effects that a second prime coat presents[5]. They discovered that the use of an additional prime coat lowered permeability by 30%. The presence of the second prime coat did not show significant differences in strength for most cases. The samples tested had only three backup coats and a seal coat in addition to the prime coat(s)[5]. The permeability drop of 30% between five and six layers shows that the added prime layer restricted gas flow more than the average of the other layers.

B. Snyder and others also did a small study on prime and intermediate coat strength. They determined that in the green state, backup coats were the strongest with prime coats being only slightly stronger than intermediate coats. Upon heating the samples the strength relationship was reversed, though the true cause of this may be hidden since the prime and intermediate layers were significantly larger than the backup

layer in that test[6]. It can be deduced from the above findings that the prime coat is a main restriction of gas flow and has limited contribution to the overall strength of the mold.

At the other end of the shelling process, M. Hendricks and others looked at the mechanical properties of the seal coat. Their testing compared the difference between backup and seal coats as well as the effects of additional seal coats and post-autoclave patching. They concluded that the seal coat aids in strengthening the mold. Compared to backup coats, the seal coat imparts a higher modulus of rupture (*MOR*), but because of the seal coat being thinner this can be misleading since the backup coat has more load bearing capacity. When neglecting the difference in backup and seal layer thicknesses, it is noticed from their results that both types of layers had the same restriction on gas flow. Their experiment also investigated the effect of a second seal coat using either the slurry viscosity of the backup or seal slurries. It was found that when applied to the relatively smooth first seal coat, the more viscous coating was thicker and restricted gas flow more than the less viscous coating. This finding is in agreement with the previously mentioned results for highly viscous prime coats, and shows that slurry viscosity has an effect on gas flow through the mold[7]. The reason for the decreased gas flow rates through the mold is because of mold thickening and water content of drying slurry. The following equation theorized by Menshikov,

$$P(S_{x,n}) \leq e^{-an} \tag{1}$$

states that as the length, *n*, of material a fluid travels through increases, the probability, $P(S_{x,n})$, of pores aligning for fluid flow decreases exponentially in relation to a material

constant, a[8]. Another factor is that more viscous slurries have a lower water to solid ratio so less micro pores are produced in the mold from water evaporation.

1.2.1.2. Layered structure. Karel Jancar did a study on manufacturing conditions of lost-wax molds back in the late 1960's[9]. His work showed that the viscosity of the coating slurry has a major affect on the coating density, shell thickness, and the resulting gas permeability. His work shows that coating density increases in a parabolic fashion with regard to slurry viscosity. When comparing molds with different thicknesses and flour grain size, a sharp drop in gas permeability as a function of mold thickness was noticed until at least 4mm of thickness was present. At that thickness the gas flux of the mold samples started to remain constant following additional thickening. When directly comparing the effect that slurry viscosity had on gas permeability, a major drop in permeability was noticed during mid-range slurry viscosities. This divided the results into what appears to be two different regions differing by more than an order of magnitude.

Work done by C. Matzek and later published by J. Niles presents some of the effects slurry viscosity and stucco size can have on the mechanical properties of investment casting molds. His work examined backup slurry viscosities in the range of 8-19 seconds on a #4 Zahn cup, and their interaction with three stucco size ranges between 16 and 50mesh. For this study, Matzek produced samples consisting of one primary, five backup, and one seal coatings. It was noted that higher viscosities, as well as larger stucco both produced thicker shells. The Modulus of Rupture (MOR) calculated was not found to be significantly different between the different samples, but the higher thicknesses did allow for a higher load capacity. He concluded that the permeability and

volumetric air flux for all the samples was also the same, but a slightly higher value (40%) was seen for the samples made from the lowest viscosity slurry (8 seconds, #4 Zahn cup).[10]

While the cause of the permeability difference in Matzek's work may not have been fully determined by him, a possible explanation can be seen in work by B. Snyder, D. Scott, and J. Snow a few years later. A side project they performed examined the effect shell structure had on mechanical properties[6]. They tested three different slurry viscosities that formed three different shell morphologies proposed by R. Doles[11]: Monolithic, Semi-layered, and Fully Layered. When comparing the viscosities used by Snyder et al and Matzek, the conclusion that Matzek's lowest viscosity produced monolithic structures while the higher viscosities were semi-layered structures. This difference in shell structure is a possibility for the differences in permeability. It was not conclusive in their study whether the shell morphology had an effect on permeability. While the monolithic structure had a higher gas flow rate than the semi-layered structure, it had nearly the same gas flow rate as the fully layered structure. In regards to strength, they noticed that the monolithic structure presented the weakest mold[6]. The weak nature of the monolithic structures can be accredited to the alignment of the stucco particles with each other. In a monolithic structure the boundaries between stucco and the surrounding media can align to form paths through the mold thickness along which cracks can propagate. In layered structures the cracks travel through the mold media but require slight direction changes to align with the boundaries when the crack reaches a plane of stucco.

1.2.1.3. Structure changes during firing. A large amount of information concerning the physical changes in investment casting molds during firing was researched and compiled by M. Hendricks[12]. Along a density-temperature curve three different stages can be observed during the sintering of ceramic molds: Initial, intermediate, and final. The mold undergoes slight densification and pore shrinkage during the initial stage. It is in this stage that ceramic grain boundaries are first defined and surface smoothing takes place. The intermediate stage is the temperature range in which the majority of densification and pore removal and isolation occur. The final stage shows little additional bonding and mainly involves the growing and combining of ceramic grains previously formed. Since the majority of permeability is lost during the intermediate stage, Hendricks proposed that during firing the shell should be heated through that stage as quickly as safely allowed, and to hold at the final stage to produce more porous strong molds. For the alumina powders tested in that research, the temperature ranges for the stages were 1300-1400°C, 1400-1625°C, and >1625°C. While Hendricks did not test other molding materials, he predicts that fused silica temperatures would be lower and zircon temperature ranges would be higher than those found for alumina.[12]

1.2.2. Mechanical Testing Methods. The most commonly used and reported measure of mold strength is Modulus of Rupture (MOR). Since shaping a sample for use in a tensile test presents too many problems and the compressive strength of ceramics are much higher than their tensile strength, a flexural bending test is preferred. This test does have limitations, which have resulted in the proposal of additional testing methods.

1.2.2.1. Modulus of Rupture Variations. The MOR test can be performed using two different types of fixtures: Three-point and four-point. The three-point bend test is most common because of its simple structure. Since it uses a single loading point at the top center of the sample, the highest stress is right below the loading point and the rest of the sample span ranges linearly from zero (at the bottom supports) to the maximum. The four-point bend test uses two equal loading points which exert a lesser stress to the sample, but apply a uniform stress profile between the loading points. This allows the four-point bend test to sample a larger area. The increased likelihood of containing a critical flaw within the maximum stress region is far higher using a four-point bend test. It is because of this that four-point bend tests will give a lower MOR value which was statistically proven by V. Richards and others.[13, 14]

A limitation to a four-point bend test is association of the deflection with the loading to generate a stress-strain curve. In addition to stress limitations, M. Hendricks pointed out in one of his experiments that mold strain behavior and MOE (Modulus of Elasticity) should also be monitored. The work represented by the area under the stress-strain curve presents the toughness of the mold and its ability to resist pressure based cracking. The strain is of importance since a mold must also maintain dimensional tolerances. Even if the mold does not crack, excessive bulging during casting can cause the casting to be rejected.[15]

The orientation of the sample in a MOR test is of importance. Bending puts the bottom half of the sample in tensile while the top half is in compression. The maximum stresses are seen at the surfaces of the sample and the center experiences no net stress. Since ceramics have much higher compressive stress limits than tensile stress limits, the

samples will always fail first along the bottom surface. This limits the test to only half the sample. While it can be argued that there is need to test the backup layers because of internal forces during pattern removal and casting, the thermal gradient stresses are more often the cause of cracks. Based on the occurrence and cases of the cracks reviewed in previous publications, G. Barnes recommended testing of the prime coat predominately and orientating that side down for bending tests[16]. This recommendation for testing the prime face of the mold was also proposed by Richards and Connin[13] based on the observed frequency of tensile fracture of the hot face (primary coat).

1.2.2.2. Alternative tests. In addition to the common MOR test, other tests based on sample shape have been proposed. Since stress is concentrated at corners, G. Barnes and P. Withey proposed a method for testing edge strength[16]. Their edge strength test used a hollow wedge shaped sample like that of a turbine blade and applied force along the inner wall using a wedge. They found that this test was a better representation for sharp cornered parts, and that for a 30º wedge the stress concentration would give half the MOR value of a three-point bend test.[16]

A method for testing both permeability and pressure limit was devised by B. Snyder and others which has gained a fair amount of support in following years[6]. They proposed the use of a hollow cylinder hooked on both ends to an air or water system and pump. By sealing one end, permeability could be obtained from the discharge rate through the mold. The same set up could be used (with the addition of a thin wax layer on the prime coat surface if needed) to perform a burst test measuring the internal pressure required to propagate a crack through the mold. Their results showed a common

trend between their pressure results and MOR results using the conventional three-point test.[6]

1.2.3. Additives. Additional materials can be incorporated into the slurry or stucco for an investment casting mold. There have been a few publications concerning the use of inorganic materials to improve strength, as well as the use of organic materials to increase porosity. A lot of this information is centered around ceramics in general, and most have little relevance to the dip coating method used for investment casting.

1.2.3.1. Fiber strengthening. The use of polymer and ceramic fibers in the slurry has been proposed as a method for increasing mold strength. Alumino-silicate fibers in slurry were tested by P. Maity up to a concentration of 0.66wt%. His testing showed a strong increase in MOR for the samples as the concentration of fibers increased. The reason he presented for the increased strength was crack growth resistance presented by the fibers. The fibers were found to lay mostly parallel to the coating layers putting them perpendicular to the direction of crack propagation.[17]

1.2.3.2. Fugitive based porosity. The use of a sacrificial fugitive is a common and cheap method for increasing porosity within ceramics. Other methods commonly used for ceramics in general are the use of granular particles, highly porous materials, gas bubbling, chemically expanding compounds, and extrusion.[18] Though other methods may produce more porosity, the methods usable for the investment casting process are limited.[18] Since the mold is created by thin layers of ceramic bonded together by dipping, most methods cannot be incorporated, and if large porosity is present during shelling it will be filled in by the liquid slurry on subsequent dips.

Commonly selected burnout materials are coke, petroleum, and polystyrene. Sacrificial additives have a limit since too much can fatally limit the amount of bonding within the mold. Though the porosity of a ceramic mold with granular structure may be high, the majority of that porosity is not open. Through the use of burnout additives the chances for the pores to be connected greatly increases. Under certain ceramic forming methods it has been possible to produce ceramics with up to 65% porosity, but this high of a value is not likely for the dip coating method.[18]

1.3. FOCUS OF RESEARCH

The objective of this research was to formulate a robust process for producing silica investment casting molds. For this objective, the term robust was regarded to be the ability to alter both load tolerance and volumetric air flow rates through the mold by controlled alterations in the process. Through the experiments, three process parameters were tested under varying levels and found to alter the desired mold properties. The three process parameters were stucco particle size, slurry viscosity, and the presence of sacrificial particles in the slurry. Those three parameters allowed the changing of layer thickness, internal mold structure, and mold porosity, which in turn control the mechanical properties of the mold.

2. EXPERIMENTAL PROCEDURES

One focus of this research has been to control permeability in investment shell molds. The mechanism for permeability through a mold is based on the presence of pore channels and how they interact with each other. For a pore channel to increase permeability it must form a continuous path from the prime coat to the seal coat. In this research, an initial method was formulated to produce a low permeability, high strength investment mold to understand the variables that strengthen the mold. Further testing examined alterations to the process to bring about controlled changes in mold structure to increase air flow through the mold.

When making process alterations to improve mold air flow, the main parameters of interest were the resulting permeability and volumetric air flux through the molds. Second to those parameters, the porosity and density of the molds were of importance because of their value in inferring internal structure. In addition to those tests, mold strength was also tested to determine the minimum number of coating layers required to withstand casting and pattern removal pressures.

2.1. SLURRY CHARACTERIZATION

The slurry used for producing investment shell molds has a major effect on mold properties. The materials used to make the slurry govern the mold's reaction to temperature changes and its rate of heat transfer from the molten metal. For these experiments, fused silica based materials were selected for both the slurry's binder and solids so that material ratios did not become a variable. This limited the primary phases

present to only amorphous silica and cristobalite depending on the temperature history of the molds.

The properties of the slurry have a direct effect on the formation and structure of a mold. The viscosity of the slurry affects the surface tension of the slurry coating the patterns, with higher viscosity slurries producing thicker slurry layers within the mold's structure. By controlling the slurry viscosity, the slurry-stucco layering was replicated nearly uniform through the thickness of all samples.

2.1.1. Slurry Preparation. The ceramic slurry to build the investment molds consisted of a mixture of fused silica flour in a colloidal silica binder. The binder used was Megasol™ which contained 45wt% amorphous silica and <1wt% sodium hydroxide in a water solution. The flour was Ranco-Sil® fused silica with a target mesh distribution of -200 and a supplier-provided sieve distribution as given in Table 2.1. The flour and binder were combined in a 2:1 weigh ratio giving a 4.44:1 solids ratio. Initial, high shear mixing of the ingredients was done using a 333rpm1/40HP, DC motor until no clumps of flour were visible. Once all the flour was adequately dispersed into the binder, the bucket was placed onto a plate rotating 15.7RPM with a scraper bar, shown in Figure 2.1, to maintain a constant low shear rate to keep the solids from settling.

Table 2.1 Supplier-Provided Sieve Distribution for Silica Flour

	USS Sieve	30	80	100	140	200	325	PAN
Grade	um	600	180	150	106	75	45	PAN
#4		0	0-0.5	0-0.5	0-4	3-9	13-20	69-81

Figure 2.1. Mixing plate and scraper bar shown with an empty mixing bucket

2.1.2. Slurry Parameter Control. After preparation, the slurry was left under low shear stirring for a minimum of 12 hours to allow air bubbles, introduced during flour addition, to float out. Once the entrapped air had escaped the slurry and the slurry's viscosity had stabilized, rheological testing was started. The viscosity of the slurry was tested using a Brookfield DV-II+ Pro viscometer equipped with a LV3 spindle operating at 30rpm, as shown in Figure 2.2. The LV3 spindle was selected because the viscosities tested were well within its testing range.

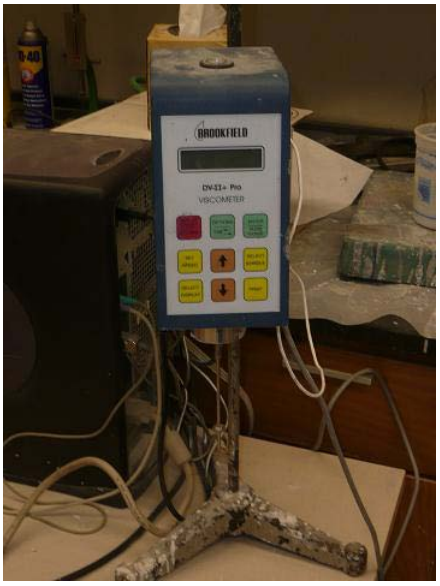

Figure 2.2 Brookfield DV-II+ Pro viscometer used to measure slurry viscosity

The readings from the viscometer under different spindle speeds were collected for slurries ranging from 50-65wt% flour. The spindle speed was cycled from 10RPM to 100RPM and back in 10RPM increments. The speed was changed instantly every ten seconds and reading were taken eight seconds after each speed change.

The viscosity readings shown in Figure 2.3 show that as the concentration of solids within the slurries increase the viscosity also increases. As the speed of the spindle increased the dynamic viscosity readings decreased. The effect of particle settling can be noticed by the difference between readings during the up and down portions of the speed cycling. As particles were allowed to settle out of suspension over the testing time, the concentration of solids in the tested area of the slurry decreased causing the viscosity to lower. During the second half of testing the 50wt% flour slurry, the dynamic viscosity of the slurry appears to decrease along with the spindle speed, but this is only because the

increase in dynamic viscosity from lower spindle speeds was less than the viscosity drop due to solids settling.

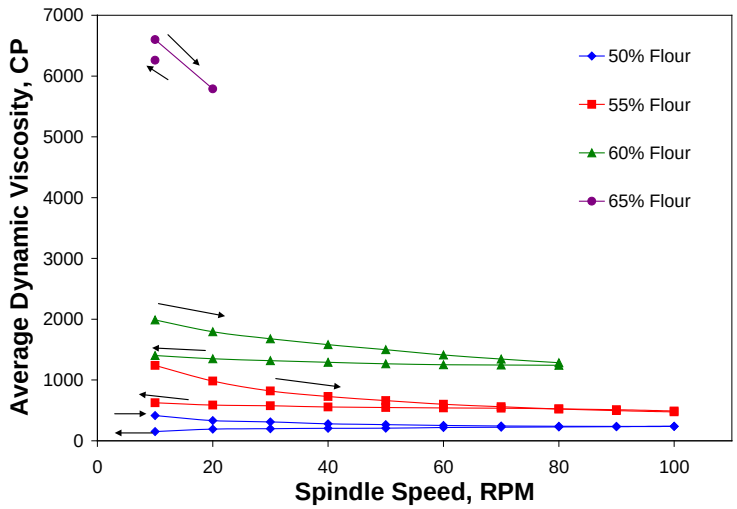

Figure 2.3 Dynamic Viscosity readings over time for different spindle speeds

As the spindle speed increased the amount of torque experienced by the spindle also increased. For the faster spindle speeds in the 60wt% solid slurry and most of the spindle speeds in the 65wt% solid slurry the torque experienced by the spindle was over its allowable tolerance setting and readings could not be collected. Since the flour content of the production slurries were going to start at 66wt% flour before being diluted with water, the findings from the 65wt% solid slurry in this experiment was used as reference for the non-diluted slurry. A spindle speed of 30RPM was selected since it was the fastest speed that would not have problems from exceeding the spindle's torque limit when testing slurry after some water diluted.

To lower the viscosity of the slurry, de-ionized water was added in controlled volumes. The added water was given a minimum of 15 minutes to disperse throughout the slurry before addition rheological readings were taken. In the event that the viscosity of the slurry was below the target range, natural evaporation was used to lower the water concentration.

The density of the slurry was monitored prior to every coating. A 100-mL graduated cylinder was used to measure out a set volume of the slurry within an accuracy of 0.5mL. A sample of slurry greater than 100mL was collected from the slurry tank using a separate container, and then transferred into the 100-mL graduated cylinder. During pouring, care was taken to minimize the amount of slurry touching the inner walls of the graduated cylinder above the 100milliliter mark. If slurry was present on the walls, it was allowed to drain down before all 100mL was added. If too much slurry was added, the excess amount was poured back into the mixing tank and the remaining slurry was allowed to drain back down off the internal walls. Any slurry on the exterior surface of the graduated cylinder was wiped off using dry paper towels. The weight of the graduated cylinder without the slurry was subtracted from that with slurry and multiplied by 10 to determine the slurry weight per liter. The use of a mud cup for controlling measured volume was considered at first, but rejected. The top opening of the mud cup was found to not be of sufficient size to allow slurries of the target viscosities to freely leave the container during closing.

2.2. PATTERNS

The condition of the pattern used in investment casting is important for the quality of the mold's internal surface and support of the mold during initial coats. The surface of the pattern is mirrored onto the interior of the mold, which subsequently is mirrored onto the casting. For this experiment the patterns used were made out of expanded polystyrene (EPS) foam. This material was selected for its ease of shaping and removal from the finished mold. The foam was removed from the mold through combustion with oxygen during the sintering process for the investment shell molds.

2.2.1. Pattern Fabrication. The patterns used to make all the test samples were formed from expanded polystyrene (EPS) sheets. The EPS sheets were produced through chemical expansion to the dimensions 15"x7"x10mm with a density of 1.5g/cc. All cuts, when shaping the foam, were done using a hot wire tool. If thicknesses greater than that of the foam sheets was needed, foam parts were attached to each other using thin layers of hot glue.

After initially considering and testing other pattern shapes the decision was made to use 7"x1"x0.4" strips of foam. This shape eliminated the use of glue and the resulting seam lines between foam pieces when thicknesses over 0.4" were used. The length of the sample allowed for the production of a 1.5" long permeability sample at the end and two MOR test pieces from the sides.

To increase the occurrence of the slurry wetting and reduce the amount of slurry draining off the pattern surface, the surface of the pattern was slightly modified. The expanded surface of the foam was too smooth in most areas to retain slurry and prevented wetting, thus requiring multiple coating attempts or the possible addition of a surfactant

to the slurry mixture. In addition to this concern, the surfaces of the patterns were not uniformly smooth because of small scratches and dents caused during shipping. Also, the surface quality of the foam was found to differ greatly from the uncut surface following cutting via a hot wire.

The surface of the foam patterns was modified using 20-grit sandpaper. The sandpaper was run across all surfaces of the foam with a 1-2lbf force exerted perpendicular to the surface. Sandpaper was run across all the surfaces three times to generate a consistent texture over all. If the use of the sandpaper created ripples or gouges in the pattern, that pattern was discarded and replaced.

The surface quality of foam patterns and their resulting prime coats were compared using a Nanovea laser surface profiler with a pen set to a range of 400um, shown in Figure 2.4. Samples with unaltered expanded surfaces, abrasively modified surfaces, hot wire cut surfaces, and surfaces coated with wax were all evaluated for differences. The results from four 10cm x 10cm regions of each sample were averaged together and are presented in Table 2.2. Although the sandpaper modified foam surface was not as flat or smooth as the unmodified or wax coated pattern surfaces, the resulting mold surface was smoother than its pattern and had a narrower height range than the other mold surfaces tested. It was because of its uniform mold surface, improvement of hot wire cut surfaces, and better wetting with the slurry that sandpaper-modified foam patterns were used for these experiments.

Table 2.2 Surface Characteristics of Pattern and Internal Mold Surfaces

		Wax Coated	Expanded	Sandpaper	Hot Wire Cut
Pattern	Sz (Height Range, um)	134.375	114.550	387.250	354.250
	Sq (Root Mean Square Height, um)	8.023	6.703	37.375	38.125
Mold	Sz (Height Range, um)	242.000	290.750	229.250	367.500
	Sq (Root Mean Square Height, um)	8.018	8.178	21.275	42.700

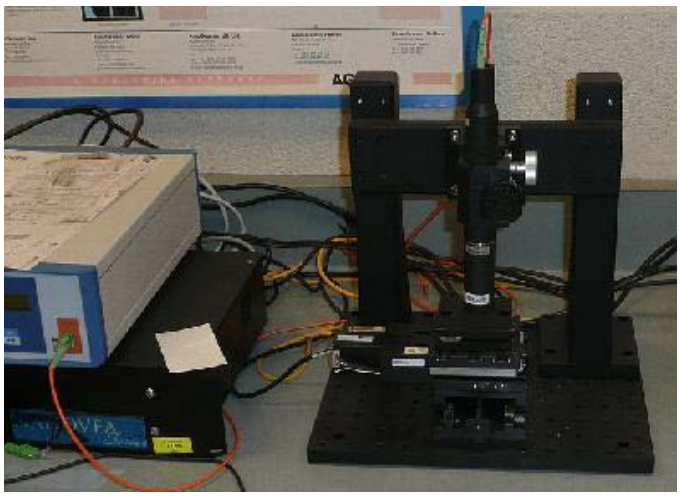

Figure 2.4 Nanovea Laser Surface Profiler used to measure surface quality of patterns, molds, and castings.

2.2.2. Pattern Coating. If the monitored parameters of the slurry were in the target ranges and the pattern/mold being coated was dry, the pattern was dipped for coating. The top inch of the patterns was used as a grip area while the rest of the pattern was submerged into the slurry for at least five seconds and rotated 360º to allow all sides to be fully coated. The pattern was then gradually removed from the slurry and

suspended over the slurry tank to allow excess slurry to naturally drain off. The patterns were held at a 45º angle to the horizontal and were rotated along their central axis at a rate near 10rpm. This rotation prevented over draining from a single edge and creating a non-uniform coating thickness across the surfaces.

Once the interval between drips from the shell exceeded three seconds or had been draining for over a minute, whichever came first, stucco was applied to the wet surface. The stucco was applied using the rainfall method, were the stucco was sprinkled onto the pattern through a grated container suspended two feet above the pattern. The pattern was rotated so that each of the five coated surfaces was in contact with the falling stucco for at least three seconds. The stuccos used were Ranco-Sil™ fused silica grades A,B, and C. The supplier-provided mesh distributions of the three different varieties are presented in Table 2.3. Except for tests in which stucco size was varied, the B range of fused silica stucco was the one applied to all samples.

Table 2.3 Supplier-Provided Sieve Distribution for Stucco Material

	USS Sieve	10	20	30	40	50	80	100	140	200	PAN
Grade	um	2000	850	600	425	300	180	150	106	75	PAN
C		0-1	80-95	2-16	--	0-4	--	--	--	--	0-2
B		--	0-1	25-35	34-48	16-32	1-8	--	--	--	0-1.5
A		--	--	--	0-0.5	3-12	--	72-87	5-16	0-3	0-1.5

2.3. TESTING PROCEDURES

2.3.1. Shell Permeability. End sections of the sample shells were cut for permeability testing. The samples were three-dimensional with simple geometrical

hollows inside consisting of either cylinders or rectangular tubes. The cut side of the sample, which was open, was closed by attaching it to a metal plate using water-proof marine epoxy. The plates used all had 3/16 inch holes in their centers for air flow and had a female pipe coupling welded on one side centered on the air hole. Marine epoxy was applied over the welds to insure that no air leaks were present. The samples were attached to the plate opposite the couplers by applying the epoxy to the cut surface and then carefully pressing onto the plate. Once on the plate, a continuous line of epoxy was applied around the sample-plate boundary. The first application of epoxy was to prevent separation of the sample from the plate during pressurization, while the second application of epoxy was to guarantee no leaks were present. The epoxy was set for at least 18 hours to allow for adequate strengthening prior to permeability testing.

Shell permeability was measured using a Simpson-Gerosa Digital Absolute Permmeter shown in Figure 2.5. Since the samples were hollow shells, and not the standard solid cylinders, a different method of attaching the samples was used. A standard hollow fixture was attached to the permmeter with a rubber stopper on top with a small hole in its center. A hose with an end attachment slightly wider than the stopper hole was inserted into the stopper to act as a connection between fixtures. The other end of the hose had a 3/8” male pipe fitting which was used to connect with the female pipe fitting on the sample’s plate. Initially, the permmeter was run without the attachment of a shell sample to determine air resistance through the fixtures and tube, and it was determined to be negligible. While performing permeability testing, the samples were unmoved and oriented horizontally. No surface of the sample was allowed to touch

another surface and the sample was horizontally symmetric to balance any effects of gravity.

Figure 2.5 Digital permmeter with attached sample used to test mold permeability

At the start of the test, the air in the fixture line and the sample was pressurized to the desired level of $10g/cm^2$. Along the sides of the air containment chamber were two markings separated by a height equivalent to 500mL within the chamber. The markings were detected by an optical sensor and the time between detection was internally recorded. Once all the air within the chamber had been expelled through the sample, the permmeter displayed the AFS permeability value associated with the recorded time and assuming standard sample dimensions. Since non-standard samples were used, the time, *t*, to expel 500mL through the sample had to be back-calculated using the following equation:

$$t = \frac{763.94}{Perm_{AFS}} \tag{2}$$

The Darcy permeability, k_D, of the samples was recalculated with the derived time, measured dimensions of the sample, and physical properties of the air used during testing, using this equation:

$$k_D = \frac{V}{t}\frac{\mu}{A}\frac{L}{\Delta P} \tag{3}$$

Where V is the percolated volume, t is the time, ΔP is the difference in air pressure inside and outside the sample, μ is the viscosity of air at 25°C, A is the internal surface area of the sample, and L is the average thickness of the sample walls taken over four locations on the sample. While permeability values are useful for material comparisons, a more useful mold parameter is the superficial air flow velocity through the mold, represented as v in the equation,

$$v = \frac{k_D}{\mu}\frac{\Delta P}{L}. \tag{4}$$

The superficial air flow velocity gives a linear rate of air movement perpendicular to the mold surface. Since equations 3 and 4 can be combined to give the equation:

$$v = \frac{V}{tA} \tag{5}$$

it can be noted that for this case the superficial air flow velocity is the same as volumetric air flux[19] through the mold. This value can then be used to determine if air is expelled from a mold as fast as metal is being added to it or if the air will become pressurized within the mold.

2.3.2. Shell Density. An Archimedes test was performed on strips of the shell material based on ASTM C20. Strips of the shell material, usually the same dimensions as for the flexural testing, were prepared for testing by heating to 130C for a minimum of 30 minutes and then allowing to cool back to room temperature. Immediately following heating, the samples were weighed to determine their dry weight without the presence of water. Next, the samples were placed within an aluminum wire cradle. The cradle was suspended from wire supports on top of a one liter beaker filled with water. The samples were allowed to hang freely in the water without coming in contact with other samples or the beaker floor or walls. Once the samples were situated, the surrounding water was heated on a hot plate to boiling, to allow for water vapor penetration into the samples' open pores. Following two hours of boiling, the heat source was turned off and the water was allowed to gradually cool back to room temperature overnight.

Without removing the samples from the water, the wire cradles holding the samples were moved to a hanging-weight scale one at a time. The differences between the submerged cradles' weight with and without the shell samples were recorded. When removing the samples, care was given to not leech water from within the sample. To do this, contact with hands was minimized to only small patches on the sides, and the

samples were hung in mid-air by plastic clamps. The samples were weighed a third time by suspending them in air while still wet.

The percent apparent porosity, *Papp*, and the bulk density (g/cm^3), *B*, in of the samples were calculated using the following equations taken from ASTM C20:

$$P_{app} = \frac{W_W - W_D}{W_W - W_S} \times 100\% \quad (6)$$

$$B = \frac{W_D}{W_W - W_S} \quad (7)$$

Where W_D is the dry sample weight, W_S is the submerged sample weight, and W_W is the wet sample weight all measured in grams.

2.3.3. Modulus of Rupture Testing. A modulus of rupture (MOR) test was also performed for all the shell compositions tested. It was important to measure the strength of the investment shells in parallel with their permeability, since a minimum strength would be required for industrial use. The measured strengths gave an indication of how many coating layers would be required with each sample composition.

The MOR of the samples was determined through three-point flexural testing. Tests were performed on an ADMET eXpert 5602 Universal Testing Apparatus, shown in Figure 2.6. Custom designed testing fixtures were assembled for this testing and are shown in Figure 2.7. Since the fixture needed to operate at testing temperatures up to 1200C without deforming, ceramic materials were used in its construction. The use of a four-point fixture was preferred over the use of a three-point fixture because it gives a

more uniform load over a wider area of the sample[14]. Although it was preferred, the four-point fixture had to be replaced with a three-point fixture because of problems and concerns that arose during use. The position of the upper supports of the four-point fixture were harder to center on the sample, especially if it required moving the fixture or was in the confined area of the environmental chamber used for elevated temperature testing. Whereas, the three-point fixture's upper support was automatically centered with the loading rod by pivoting. The four-point fixture was also found to not be of a durable design since two of them cracked due to conveying forces.

Through preliminary testing, it was determined that a bottom fixture span length of at least three inches would be required to prevent samples from exceeding the 50lbf capacity of the load cell during testing at room temperature. Following the cutting to create the bottom fixture, the resulting span length for all tests was 77mm. The width of the test samples was targeted to be between 22mm and 33mm following cutting. Sample thickness was unaltered and varied naturally based on the number of coating layers applied. Since the structure of the shell was not monolithic, the resulting strength would have been dependent on the type of layer exposed to the surface. In addition, if the cut were through a stucco layer the removal of stucco particles from the shell would leave large holes in the surface resulting in crack initiation voids and present a lower strength.

Figure 2.6 The flexural testing apparatus used to collect loading and displacement data

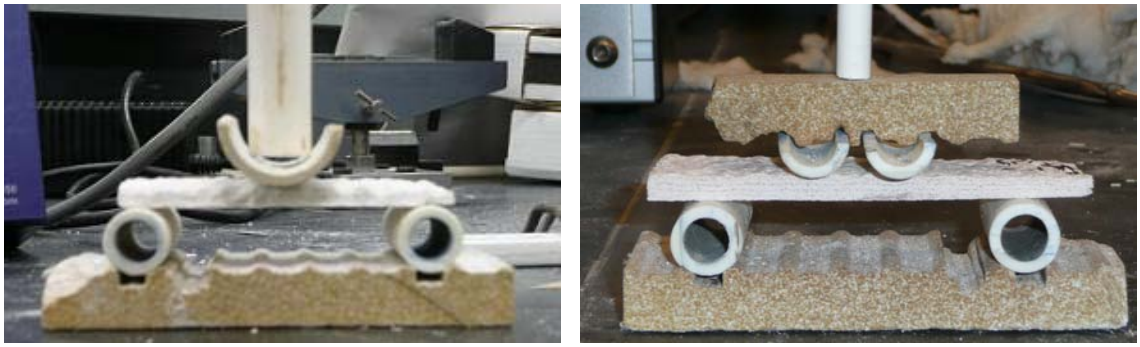

Figure 2.7 Three point and four point fixtures created for flexural testing

The controller for the flexural test was set so that the loading rod would initially have a downward velocity of six millimeters per minute until 0.1N of counter-force was exerted by the sample. Once the sample was detected, the velocity of the loading rod was halved to a constant three millimeters per minute for the remainder of that test. The amount of force applied to the sample along with the linear deformation at the center of

the sample were recorded at a rate of 60Hz until the sample failed by crack propagation through the entire thickness.

The results of the flexural tests were evaluated through three different parameters. The flexural stress on the shell and the adjusted fracture loading (*AFL*) were both calculated based on the test loading and the dimensions of the test sample. The other parameter of interest was the flexural modulus exhibited by the investment shell samples.

2.3.3.1. Flexural strength. The flexural stress, s, of samples was calculated using one of the two following equations, depending on whether a three-point (equation 7) or four-point (equation 8) flexural test fixture was used during testing:

$$\sigma_{3pt} = \frac{3PL}{2bd^2} \tag{8}$$

$$\sigma_{4pt} = \frac{3PL}{4bd^2} \tag{9}$$

In the above equations, *P* is the loading force applied, *L* is the span length between the two lower supports, *b* is the sample width, and *d* is the thickness of the sample. The flexural strain, e_f, was required for comparison with the flexural stress during plotting of stress-strain curves. For this value the following equation was used:

$$\varepsilon_f = \frac{6Dd}{L^2} \tag{10}$$

The flexural strain equation referenced the same dimensions as its paired flexural stress value, plus the inclusion of *D*, the maximum deflection along the sample's length at that point in time. The flexural modulus, E_f, is a measure of the level of flexural stress required to cause a given amount of flexural strain. This value is equivalent to flexural stress divided by the matching flexural strain, and can be simplified to the following form:

$$E_f = \frac{L^3 m}{4bd^3} \tag{11}$$

with *m* being the initial slope of the load-deflection curve.

2.3.3.2. Adjusted fracture load. The Adjusted Fracture Load (AFL) is another measure of flexural strength that has been used by some groups recently[15]. It is similar to the flexural stress calculation, but differs by not factoring in sample thickness. This is of use when the structure of a tested material is not uniform throughout. Although the thickness of an investment casting mold can be increased both through increases in coating thickness and through increases in the number of coating layers, those methods do so by altering the layering structure in different ways. Because of this, the un-cut thickness of a sample is not a directly controlled variable and is instead a product of the slurry pickup during coating, the stucco particle size, and the number of coating layers. Those three characteristics of the mold are thus more descriptive of the mold and its layering than thickness, and it allows for reproduction of samples and results. Additionally, the AFL directly relates to the performance characteristics of interest during casting and pattern removal.

The equation for AFL is:

$$AFL = f \times \sigma \times d^2 . \quad (12)$$

The flexural stress, σ, is the same as from equation 7 or 8, d is the sample thickness, and *f* is a constant factor used to normalize the AFL value. While the unit for AFL is force, it does not have a direct physical meaning. The AFL value is a reference for comparing relative load capacity between multiple samples. This makes it easier to compare differently processed molds in regards to load carrying capacity during pattern removal and pouring.

2.3.4 Burst Testing. The strength of the investment shell mold samples was initially determined by burst testing in addition to MOR testing. Unlike the MOR test, a burst test was able to test an entire sample as long as it could be sealed. Also, MOR tests ideally test a one-dimensional sample by applying a point load, whereas burst tests take a sample's three-dimensional geometry into affect. It was because of this difference that burst testing was initially done to determine stress concentration magnitudes along edges and corners and to establish pressure limitations of the samples instead of just point load limits.

Testing was performed following permeability testing. The sample attachment for the burst test apparatus was designed to connect with the same coupler used for the other test. The testing apparatus consisted of a water holding tank connected by a hose to an electric pump, set at 1/2HP and pressurizing up to 180psi, followed by a control valve, pressure gauge, and the sample attachment, all shown in Figure 2.8. During testing the

sample holder was supported over a plastic bowl which was used to collect broken pieces of the sample and the water used.

Figure 2.8 Burst test apparatus used to test internal pressure limits on three-dimensional samples.

The sample holder with the sample attached to it was connected to the burst test's sample attachment. The control valve in the hose was closed and the pressure gauge was turned on and zeroed. The water pump was turned on and the water pumped was circulated back into the holding tank through a pressure relief loop. To start the test the control valve was slowly opened, allowing water to flow to the sealed sample. As the control valve was turned, more of the water pressure generated by the pump was applied to the sample until its limit was reached. Once the sample was cracked, the control valve was again closed and the maximum pressure registered by the pressure gauge was

recorded. The location of the crack(s) on the sample was noted and the sample was then pried off of its holder and the holder was cleaned of epoxy.

In the event that the sample did not crack, but instead the epoxy sealing it to its holder was ruptured, the sample was set aside for re-testing. The epoxy was dried using a paper towel and air. After drying, additional epoxy was applied to seal the hole generated by the testing. That addition was given an additional day to set before testing was attempted again.

3. EXPERIMENTAL PROCESS AND RESULTS

Experiments started with the task of developing a process for producing slurry to test. Once a slurry procedure was determined, different coating materials and slurry conditions were investigated. In the final stage of the research, alterations to the base slurry were performed to alter mold properties further.

Most of the results were taken from testing small test samples which were produced. In addition, to the testing described in the previous chapter, plate molds were periodically produced to determine if their properties were adequate for the casting of steel.

3.1. PRELIMINARY SLURRY TESTING

Based on the few slurry parameters recorded in technical journals, the initial slurry composition was set at a 2:1 ratio between flour and binder and targeted loosely to have a dynamic viscosity of 800cP at a shear rate of 30rpm with a L3 spindle. The first combination of commercially available materials, consisting of fused silica flour (Teco-Sil®), zircon flour, and colloidal silica binder (Megasol™), proved to not be a stable suspension using the constructed mixing equipment. This suspension instability leads to the first minor testing of this research.

3.1.1. Slurry Materials. Two different commercially produced colloidal silica binders were selected as well as two commercially distributed brands of fused silica. The binders, Megasol™ and Primcote®, differed in additives and resulting pH as shown in Table 3.1. The flours compared Ranco-Sil™ #4 and Teco-Sil® primarily differed in

pH. Each of the four pairings was produced using the same flour to binder ratio and to a quantity of 750-1000g. The sample slurries were mixed in a 20oz cup under constant low speed stirring for 24hrs.

Table 3.1 Properties of Slurry Materials

Material Type	Trade Name	pH (average)	% Amorphous Silica	Other Additions
Binder	Megasol	9.5	10-50%	<1% Sodium Hydroxide
	Primcote	10.6	<50%	<10% Dipotassium Flourescein <10% Oxirane Polymer
Flour	Ranco-Sil	6.5	>80%	<0.75% Cristobalite
	Teco-Sil	5.7	>99%	<1.0% Quartz

After the degassing period, the slurry was first inspected to determine if settling had occurred. It was found that the original combination of Megasol™ and Teco-Sil® failed to keep flour particles in suspension for over a day. The opposite pairing of Primcote® and Ranco-Sil® produced slurry which was too thick to be used even after attempts at diluting the mixture were made. The other two pairings appeared to be well mixed with even flour dispersal throughout. The main factor in whether the binder and flour worked together appeared to be their combined pH. The pairing of the lowest pH materials presented a slurry which did not keep particles in suspension, while the pairing of the highest pH materials gave a slurry that thickened.

When comparing the dip coat thickness from each slurry batch, the Primcote®-Teco-Sil® slurry yielded a thickness of 23mil which was over three times that of the Megasol™-Ranco-Sil® slurry which was 7mil. Since the coating thickness produced by

mixing Primcote® and Teco-Sil® was determined to be too thick and would require large additions of de-ionized water to lower it, the other slurry was selected for further testing.

3.1.2. Dry Time. The next preliminary test was to determine the necessary drying time between coatings. Slurry of the newly re-selected flour and binder were mixed in a 2:1 ratio and then a foam strip was coated without stuccoing. The weight of the sample was monitored over the following hours and it was determined that by 3hrs after dipping the single coating was dry based on the plot in Figure 3.1. Since previous coatings re-hydrate upon future dips, it was determined that while a minimum of 3hrs was needed for the prime coat, backup coatings would require longer. Because of this fact the minimum drying time for backup coats was selected to be 4-5hrs depending on the mold thickness.

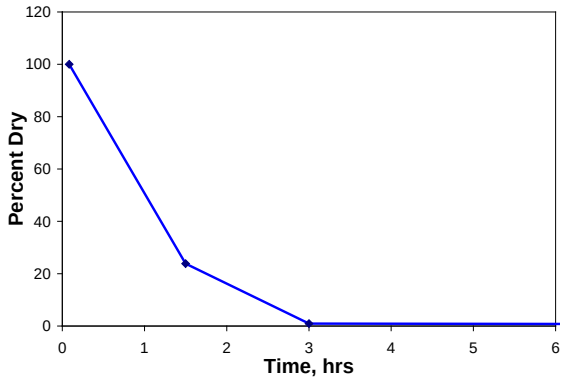

Figure 3.1 Drying rate of a single coating layer based on initial and 24hr weight

3.1.3. Initial Sample and Test Selection. The first procedural development was with the initially proposed coating method and to determine the best shape for the foam, sample patterns. The slurry for this test contained equal weights of colloidal silica,

fused silica, and milled zircon. The prime coat was applied when the slurry had a dynamic viscosity of 1050cP and subsequent coatings were applied at viscosity values between 700-900cP. Upon each coating +30-50mesh fused silica particles were applied as stucco. A single prime coat was followed by five back-up coats and a seal coat, for a total of seven coating layers.

Two different pattern shapes were selected for making the permeability and burst test samples. One pattern type was a rectangular tube with a square face of 1.2in length sides. The other pattern type was a cylindrical tube with a face diameter of 1.2in. The permeability readings for all the test samples were converted to volumetric air flux through the sample so that the differing shapes were not a factor when pooling results. The average volumetric air flux of the test samples for this experiment was 0.130mm/s with a standard deviation of 0.018mm/s. Though the different shapes were assumed to present the same mold permeability, test samples from the rectangular patterns tended to be slightly higher. This slight shift is assumed to be caused from difficulties coating corners which were only present in the rectangular shaped test samples.

3.1.3.1. Room temperature and elevated temperature flexural testing. Two rectangular test samples were cut from each of the mold samples made for flexural testing. The pairings from all the mold samples were divided evenly between two groups, which underwent the same firing conditions. One group was tested at room temperature and the other group was tested at a temperature of 1200C to simulate conditions possible during steel casting.

The room temperature test samples gave an average strength of 7.29MPa which varied by a standard deviation of 0.77MPa and is equivalent to an AFL of 249N. The hot

temperature test samples displayed one of two different responses to flexural testing. The samples either displayed plastic deformation during the test or remained rigid and attained a much higher loading capacity. The test samples which deformed only experienced a flexural stress of 4.7MPa (AFL of 183N) before their deformation put them into contact with the testing fixture. The samples that remained rigid during testing tolerated a much higher stress value averaging at 16.6MPa (AFL of 571N).

Upon examination of the testing log, it was found that all the samples which remained rigid during testing were the first samples tested that day which allowed them to increase from 23C to 1200C at the same controlled rate as the environmental chamber. The subsequently tested samples were inserted into the chamber while the internal air temperature was elevated between 400C and 600C. It is assumed that the sudden and steeper heating rates for the secondary test samples gave them a different phase constitution than those that were tested first. The more gradual first samples would have had sufficient time to start converting into beta cristobalite, but the faster heating rates of the second samples may have caused that transformation to be skipped and the amorphous silica present instead started to soften upon nearing its melting point.

3.1.3.2. Geometric force concentration. A major focus of performing burst testing on the mold samples was to determine the strength of the mold along different geometric features. The rectangular test samples allowed for testing of corners, while the cylindrical test samples tested edges. Both features are regions of stress concentration, so crack initiation was predicted to occur at a corner if present or an edge if no corners were included. Though some cracking was present upon the faces of the test samples, all samples displayed straight cracking along edges. The single circular edge in all

cylindrical samples was cracked completely around and at least three of the connected edges of the rectangular samples were completely cracked in a straight line. Examples of cracked test samples of both shapes are shown in Figure 3.2.

(a) (b)

Figure 3.2 (a) Rectangular and (b) cylindrical test samples after burst testing

The maximum pressure loading for each shape differed greatly. The edge of the cylindrical samples was capable of withstanding an average pressure of 154psi with a standard deviation of 14psi. The corners of the rectangular samples were significantly weaker in strength showing an average maximum pressure tolerance of only 31psi varying by a standard deviation of 4psi. These results show that because of significant stress concentration, in addition to difficulties coating corners, mold corners can be

expected to support only 20% as much pressure as edges, which are still weaker than flat surfaces.

3.1.3.3. Finite element analysis and high temperature prediction. Non-linear finite element models of the two burst test shapes were constructed for further analysis. The use of computer simulation helps in determining the areas of highest stress concentration and after verification with laboratory results can be used to predict pressure tolerances for mold conditions at experimentally difficult conditions, like being at 1200°C. Since the way that the flexural samples behaved in response to loading pressures were different, two different material models were considered for the simulation.

For simulation of a room temperature mold, a brittle material model was selected[20]. The use of a brittle material model assumes discontinuous macro-cracks form in the mold and are the cause of failure, which matches with what was seen during flexural testing. The relationship between stress and strain along the crack interface was governed by the following formulas:

$$d\sigma = \left[D^{el} - D^{el}T\left(D^{ck} + T^{T}D^{el}T\right)^{-1}T^{T}D^{el}\right]d\varepsilon \qquad (13)$$

Where $d\mathsf{s}$ is the stress rate, $d\mathsf{e}$ is the strain rate, D^{el} is the isotropic linear elasticity matrix, D^{ck} is the diagonal cracking matrix (which changes based on the state of existing cracks), and T is the transformation matrix (which consists of the direction cosines of local cracking coordinates).

The simulations for 1200°C molds used an elasto-plastic material model. This material model was selected since the flexural test samples displayed some ability to deform without macro-cracks extending through the entire test sample causing failure. Since the final cause of failure for the elevated temperature flexural test samples seemed to be from tearing, the simulation model for this material primarily focuses on strain levels for failure. The total strain e is defined as:

$$\varepsilon = \varepsilon^{el} + \varepsilon^{pl} \tag{14}$$

Where e^{el} is the elastic strain and e^{pl} is the plastic strain. Since the elastic behavior model of the material is linear and isotropic it is equated to the total stress, s, and D^{el}, by the equation:

$$\varepsilon^{el} = \sigma / D^{el} \tag{15}$$

For the plastic behavior of the material, the Ramberg-Osgood model was used, which gives the following relationship:

$$\varepsilon^{pl} = (\sigma / K)^{1/n} \tag{16}$$

where K and n are material constants.

Since the materials being simulated are non-linear and a large number of modeling elements were required, the use of the commercial finite element code

ABAQUS/Explicit was selected for use. To allow for finer element meshing and increased accuracy, the mold shapes were divided along planes of symmetry and only a quarter of the shell was modeled. Along the symmetry plane, boundary conditions were set to allow for displacement of the model along that plane but restricting moment force bending. For the model edges which associate with the cut edges of the mold, neither movement nor bending was allowed. The dimensions of the models were based on average mold lengths. The upper faces of the cylinders remained as a 1.2x1.2in square and a 1.2in diameter circle for the internal surfaces. The height of both cylinders was set to a length of 2.86in on the inside and the wall thickness was keep at a constant 0.23in along the enter model.

The models were meshed into 8-node brick elements. Since failure was predicted to originate at the upper corners, a finer scale of mesh as used in that region. To prevent a shear-locking problem which can happen with this type of element, a reduced integration strategy with hourglass control was implemented. The physical material properties for the two different mold materials were set to match with the average values from flexural testing, which are compiled in Table 3.2.

Table 3.2. Material Properties of Molds for Pressure Simulation

Temperature [°C]	Density [lbs/ft^3]	Young's Modulus [ksi]	Failure Stress [ksi]
20	113.4	101.5	1.22
1200	113.4	101.5	1.57

The stress distribution through the models just before failure is shown in Figure 3.3. In the square faced mold, it was that the region of maximum stress was at the rigid

fixed corner and the stress concentration continued along the edge. The circular faced mold, which did not have edges connected along that surface, displayed a concentration of stress along the edge between the side wall and end face. Along the cross-section boundaries of the models, it can be seen that the stress builds up along the inner surface of the mold edges, while the outside of the mold only has minor stress increases between edges where bowing happens. The areas of stress concentration were independent of the temperature of the mold. The only effects of the different material properties were an increase to the maximum failure stress and a slight increase to model strain deformation.

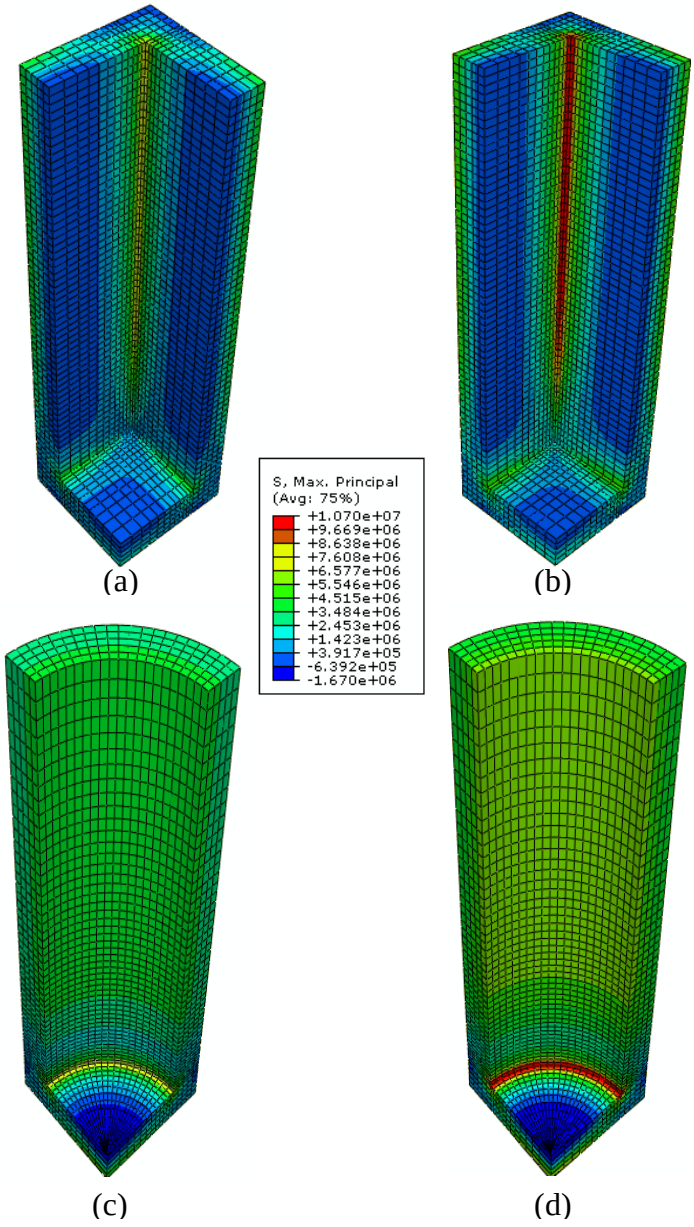

Figure 3.3 Stress distribution at failure for square (a&b) and cylindrical (c&d) models at room temperature (a&c) and 1200°C (b&d)

The maximum pressure tolerance from the simulations along with the matching results from bursting testing is given in Table 3.3. Through simulation it was found that by increasing the mold temperature to a uniform 1200°C the pressure tolerance of the

mold can be improved by approximately 37% of the room temperature limit. Both the measured results from experimental testing gave values approximately 30kPa less than the simulation predicted values.

Table 3.3. Comparison of Simulated and Experimental Burst Pressures

Shell Shape	Temperature [°C]	Burst Pressure [psi]	
		Predicted	Measured
Square Faced Prism	20	63	31
	1200	87	---
Circle Faced Prism	20	186	154
	1200	254	---

A major reason for the lower test values is from uneven shell thickness and structure. While the simulation assumed a constant mold thickness along all surfaces, this does not tend to be the case for real molds. Corners oriented upward drain slurry at a faster rate than flat surfaces, and downward corners are where slurry runoff collect before dripping. Even when trying to balance draining and build up on corners, the slurry that ends up moving there is assumed to have a lower solids rate than the rest of the slurry. This assumption is based on the fact that slurry with fewer solids has a lower viscosity and that less viscous fluids move more readily towards low points of the mold.

Another factor that causes edges and corners to have weaker and thinner structures is increasing surface area during coating. While flat surfaces have a constant surface area, the area across edges and corners increase with each coating layer. The stucco particles which contribute the most in increasing thickness are bonded on the lower layer and create the surface for the next slurry layer. Along edges there is only a

limited amount of surface for the stucco particles to adhere to, but the resulting surface area for the next layer must be greater. A diagram illustrating this coating difference is presented in Figure 3.4. This difference in area results in decreased stucco volume density on corners and edges leaving more volume containing the weaker dried slurry and more paths through which cracks can propagate.

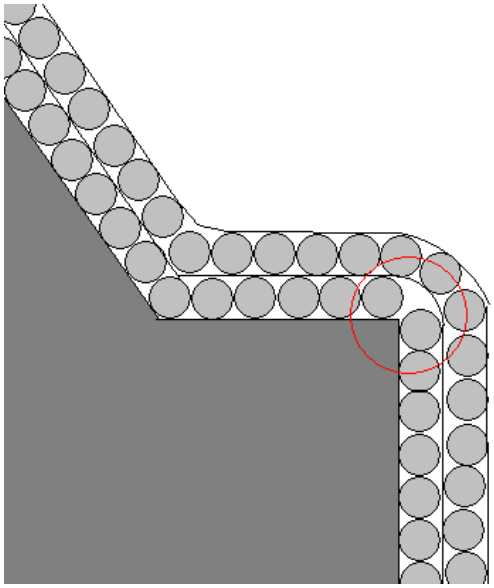

Figure 3.4 Diagram of stucco placement along corners.
A corner where stucco coating was limited is circled in red.

3.2. COATING VARIATIONS

Having usable slurry only addressed selection concerns regarding flour and binder. The other important material issue, stucco selection, had to wait until coating test samples started. The variables that were selected for this batch of test samples were:

stucco particle size distribution, number of coating layers, and the presence/absence of stucco upon a layer.

Standard slurry with a 2:1 weight ratio between the fused silica flour and colloidal silica binder was used for dip coating. The dynamic viscosity of the slurry was adjusted to 700-900cP prior to each coating dip. Half the test samples had -100+200mesh granular zircon used as stucco for the prime coat, while the other half did not have stucco applied to the prime coat. The test samples were further divided into four groups with each having -30+50mesh fused silica, -50+100mesh fused silica, -100+200mesh zircon, or nothing applied as stucco upon each backup coating. After five backup coatings were applied to the mold samples, half of each group had a seal coat applied, while the remaining half had three more backup coats applied before a seal coat. After drying, the mold samples were fired to 1000C for two hours and then cut into test samples. A summary of the testing matrix used for this test is shown in Table 3.4.

Table 3.4 2x4x2 Experimental Matrix

Variation Number	Secondary Layers	Stuccoed Prime Coat	Back-up Stucco Size
1	5	no	none
2	5	no	-50+100 mesh
3	5	no	-30+50 mesh
4	5	no	-100+200 mesh
5	5	yes	none
6	5	yes	-50+100 mesh
7	5	yes	-30+50 mesh
8	5	yes	-100+200 mesh
9	8	no	none
10	8	no	-50+100 mesh
11	8	no	-30+50 mesh
12	8	no	-100+200 mesh
13	8	yes	none
14	8	yes	-50+100 mesh
15	8	yes	-30+50 mesh
16	8	yes	-100+200 mesh

3.2.1. Permeability of the Combinations. The air flow rates through the test samples did not differ much from each other, as seen in Figure 3.5. The test samples without stucco applied to the coatings showed the lowest volumetric air flux, but also had the greatest variability because the smooth coating surfaces did not allow for proper subsequent coating and air bubbles occurred more frequently. The large -30+50mesh stucco used produced test samples with slightly higher volumetric air flux, but the difference was minor.

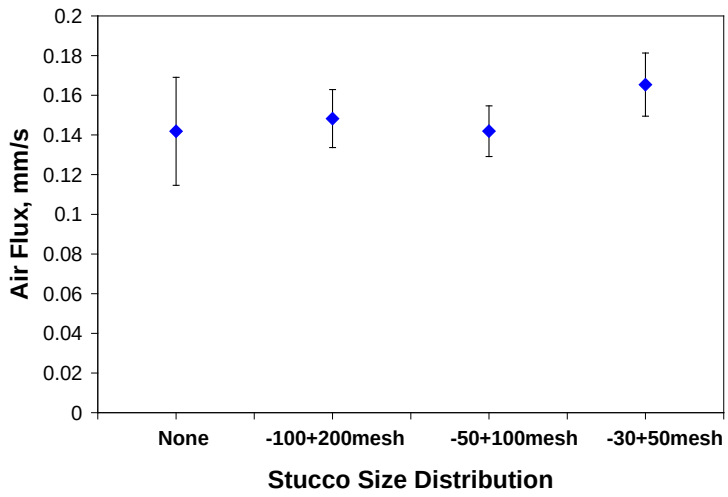

Figure 3.5 Air flow rate through molds with different sized stucco particles

3.2.2. Flexural Strength Using Different Size Stucco Particles. The maximum load which the test samples could support before failure increased as the size of the stucco particles increased, as presented in Figure 3.6. In addition to presenting higher strength for a given number of coatings, the use of larger diameter stuccos also gave increased load strength with additional coatings. As shown in Figure 3.6, having five layers using -30+50mesh stucco gave nearly the same maximum adjusted fracture load as eight layers of -200+100mesh stucco, allowing for desired strengths to be reached with far fewer coatings.

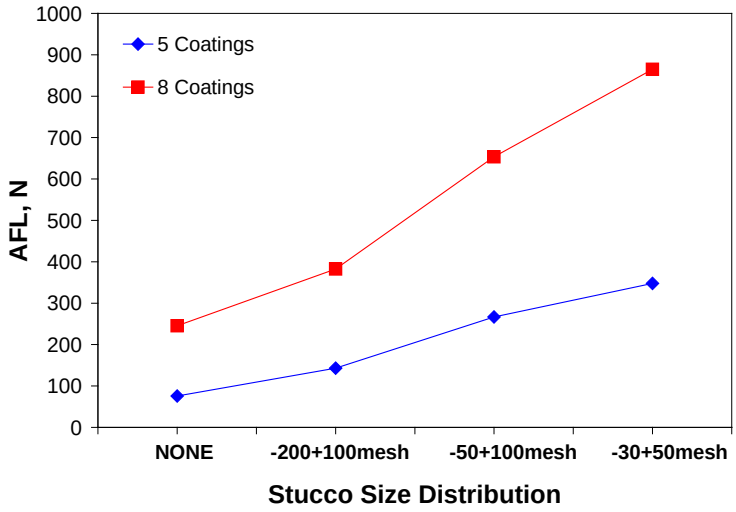

Figure 3.6 Changes in loading strength with regard to stucco size and coating number

3.3. FIRST CASTING TRIAL

Using the findings of the previous test, steel casting molds were made to determine the adequacy of the basic process presented earlier in Section 3.1 of this thesis. To do this, two separate mold types were selected for initial studies. Both mold patterns were designed for plate castings, with one having a bottom filled vertical plate with a large top riser and the other having a vertical and horizontal plate both feed from a side riser. The single plate design was used first for verifying the flow pattern of molten steel inside and to measure temperature changes in the steel and mold. The dual plate design was used for the subsequent steel heat to measure temperatures in a revised method and to observe the surface quality of the casting along differing orientations.

3.3.1. Flow Verification. A benefit of using sacrificial patterns is that testing equipment can be put inside it before molding and easily remain following pattern removal. By taking advantage of this, 16 gauge steel wires were inserted into the foam pattern at selected locations. The 56 wires were positioned through the pattern's plate in

0.5inch spacing giving a 7x8 array. In addition to these four additional wires were positioned within the runner between the sprue and plate. Centered directly below the sprue was a 12 gauge steel wire.

The wires were threaded through the foam pattern with one end bent to secure its location, as shown in Figure 3.7a. The width of the bends was restricted to 0.25inch at most so that no contact would be possible between neighboring wires. The other end of the wire was left straight and extended a minimum of 1.5in from the foam surface to guarantee about one inch of length was exposed from the final mold surface. Prior to coating the pattern, electrical tape was used to cover around 0.75in of the wire ends. Electrical tape was used because its smooth surface did not retain slurry coating easily. When slurry did remain on the electrical tape, it was removed by flexing the tape prior to each subsequent coating dip. Once the mold shown in Figure 3.7b was completely coated and given a final drying period, the electrical tape was removed from the wires and the mold was fired to 1000C for two hours for complete foam removal. Each of the 16 gage wires were individually connected to strands of standard 16 gauge electrical wire, as shown in Figure 3.7c. These wire strands were connected to a 64 channel data acquisition system, set to record at a rate of 100hertz. The single 12 gauge wire at the sprue base was attached to a separate 12 gauge electrical wire and connected to a 5V power source present in the data acquisition system.

(a)

(b)

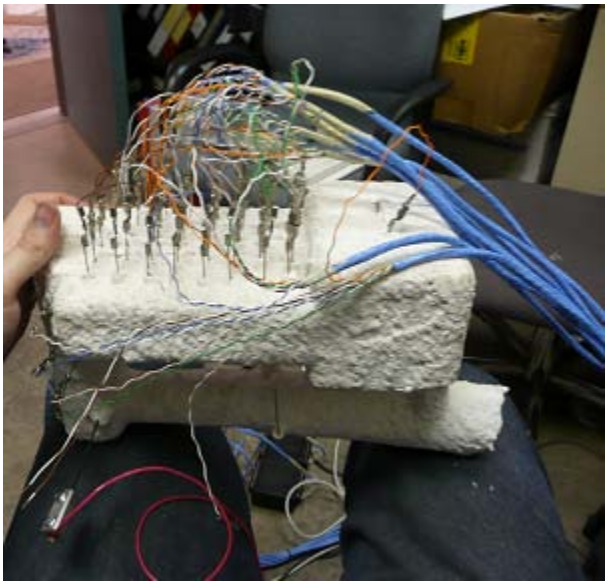

(c)

Figure 3.7 Pattern for filling analysis (a) before molding, (b) after molding, and (c) after wires were connected to the data acquisition system.

The idea behind this method was to introduce a small electrical current into the molten steel once it reached the base of the sprue. The data channels connected to the 16

gauge wires would have read only an ambient static signal while the mold is empty, but that reading would be replaced by an actual electric signal once the wire contacts the molten steel. The signal responses were analyzed following the heat and the time stamps when each channel's signal changed was recorded and assigned to the matching location on the mold as an indication of fill.

The results of this test were compared with those generated using a three-dimensional finite element computer simulation. The simulation consisted of an initially empty mold that was filled with melted steel entering the mold in a 25mm diameter stream at a constant pressure of 1000mbar. The cubic element cells in the simulation mesh were setup to monitor velocity, temperature, and pressure for the air and steel within the mold, and the temperature within the mold. Between each time step during the simulation, the density and viscosity of the materials were updated to match the current temperature of the material. To perform this simulation the commercial application MAGMAsoft was used since it can easily monitor the desired parameters and adjust material properties to match current temperatures.

The dimensions of the single plate pattern were used to create a computer model of the casting volume. The outer mold was automatically generated around the casting volume assuming a uniform thickness of 6.4mm. For initial study, the mechanical and thermodynamic properties in the simulation were approximated using recorded material properties for silica sand and steel with a chemical composition given in Table 3.5. Through subsequent thermodynamic and fluidity testing, the material properties in the simulation database were updated to better reflect the actual materials in use.

Table 3.5 Chemistry of Referenced Steel

C	Si	Mn	Cr	Ni
0.22	0.30	0.40	1.0	3.0

Before mold filing was simulated, control points were incorporated into the computer model matching the positions of the wires in the physical mold. The control points were set to monitor both air and metal pressure at the assigned locations. Following the simulated filling of the mold, the pressures were monitored, with respect to casting time, in the same way that voltage signals were monitored in the physical mold. The times at which steel reached each control point was defined as the first recorded time when air pressure became zero and the metal pressure became non-zero in the data log. When the time values of both actual and simulated tests were standardized with each other using the first wire/control point in the runner, it was possible to do a paired comparison between the two in Figure 3.8.

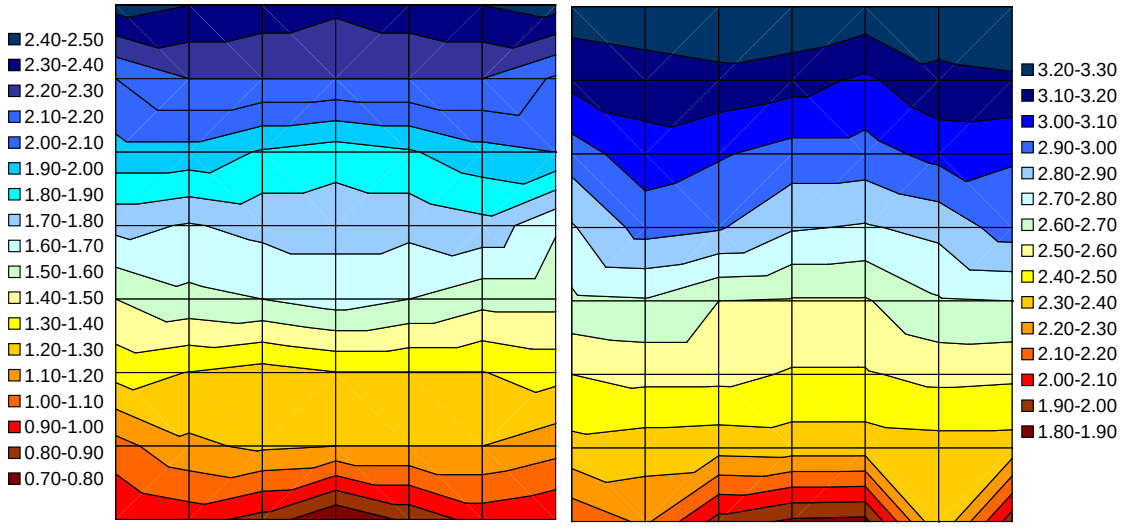

(a) (b)

Figure 3.8 (a) Simulated and (b) casting filling times shown in 0.1sec increments across the tested region of the plate

3.3.2. Measuring Temperature Profiles. The first attempt to measure the thermal history of the mold and the cast steel during casting used standard thermocouples with the wire contained in a U-shaped quartz tube. The quartz tubes of the thermocouples were inserted directly into the sides of the foam pattern while their ceramic bases were left outside to become part of the mold. Similar to the wires for the filing analysis, the external leads of the thermocouples were covered in electrical tape to prevent slurry from building up on them. Due to concerns about safe maximum temperatures for the thermocouple insulators during mold firing, the firing temperature of this mold had to be lowered to 600C to prevent damage to the thermocouples. Upon trying to pour steel into the mold, it was discovered that residue from the pattern materials, as seen in Figure 3.9, was still present deep in the mold. This residue completed burning when the high temperature of the liquid steel was introduced and the resulting gases prevented the majority of the steel from entering the mold.

Figure 3.9 Pattern residues are observed inside of the mold that would not allow filling

Thermal analysis of the mold and steel was again attempted for the next heat. For this attempt, the choice in thermocouples was changed to using ceramic cased thermocouple wires that would tolerate the desired maximum firing temperature. The smaller size of the newly selected thermocouples allowed them to be placed within the mold. Three thermocouples were added to the mold every two coating layers with the first being after the prime coat. The thermocouples were attached by orientating the dry mold so the thermocouple was on top and then applying a small amount of slurry over the thermocouple to hold it in place until the next coating could be applied. An additional one hour was given for the slurry on the thermocouple to dry before coating resumed.

3.3.3. Casting Soundness. During the second heat, additional dual plate molds were cast without thermocouples for the purpose of determining the ability of the

molds to be filled properly. Upon removal of the molds, it was found that air had been entrapped within the casting. The upper surface of the top horizontal plates, like the one shown in Figure 3.10, was not completely filled in even though sufficient casting pressure and temperature was given. It was also noticed that some of the vertical plates also had problems with air. This problem displayed itself as surface porosity located in the far upper corner. It was determined that this porosity was caused from air entrapment and not shrinkage porosity since the porosity extended to the casting surface and solidification simulations had been used to design the risers of a sufficient size to prevent porosity in the plates.

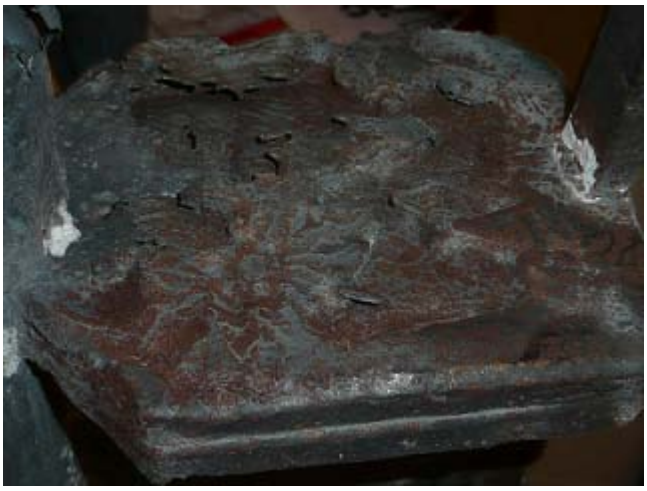

Figure 3.10 Top surface of the upper plate did not fill because air entrapment

It was determined that the molding process used to build these molds gave adequate strength to prevent cracking from pressures but did not produce sufficient means for gas removal. Upon receiving and testing mold test samples from an industrial

company, it was observed that the molding process used in the lab gave samples that were much lower in permeability than those from the industrial company. This test along with the comparison with an industrial sample showed that the focus of this research needed to concentrate on altering the molding process to improve mold permeability, even at the expense of lowering the current strength.

3.4. ALTERING MOLD STRUCTURE USING SLURRY PARAMETERS

Visual inspection of the previously built mold samples showed a completely layered structure without stucco layers coming in contact with each other. The area separating the stucco layers consisted of the hardened slurry material which presented minor permeability because of dense packing. To reduce these thick layers of low permeability the dynamic viscosity of the coating slurry was altered to give different coating thicknesses.

For this experiment the viscosity of the slurry was adjusted to different consistencies to alter the thickness of slurry picked up per coating. Upon lowering the slurry coating thickness below an undetermined threshold, the layered mold structure was expected to be replaced with a monolithic structure. Percolation Theory states that a volume's total permeability can either increase or decrease when the volume is increased. How the permeability changes is dependent on the density of the material's open porosity and whether it is higher or lower than an unknown limit. To determine if the percent porosity was above or below this limit, samples with different numbers of coatings were collected to monitor changes when increasing mold thickness.

3.4.1. Mold Structure Observations. The structure of the mold across layers was observed directly under low magnification visual inspection and indirectly by determining the open porosity and bulk density of the test samples.

3.4.1.1. Visual Observations. With unmagnified visual inspection of the test samples it was obvious that a difference in structure existed between those made from the lower viscosity slurries and the higher viscosity slurries. By observing the placement of stucco particles and the amount of material between them, three types of structures can be noted. For reference, photographs of the sample cross-sections are presented in Figure 3.11, where the stucco particles are shown as gray and the bound flour material appears whiter.

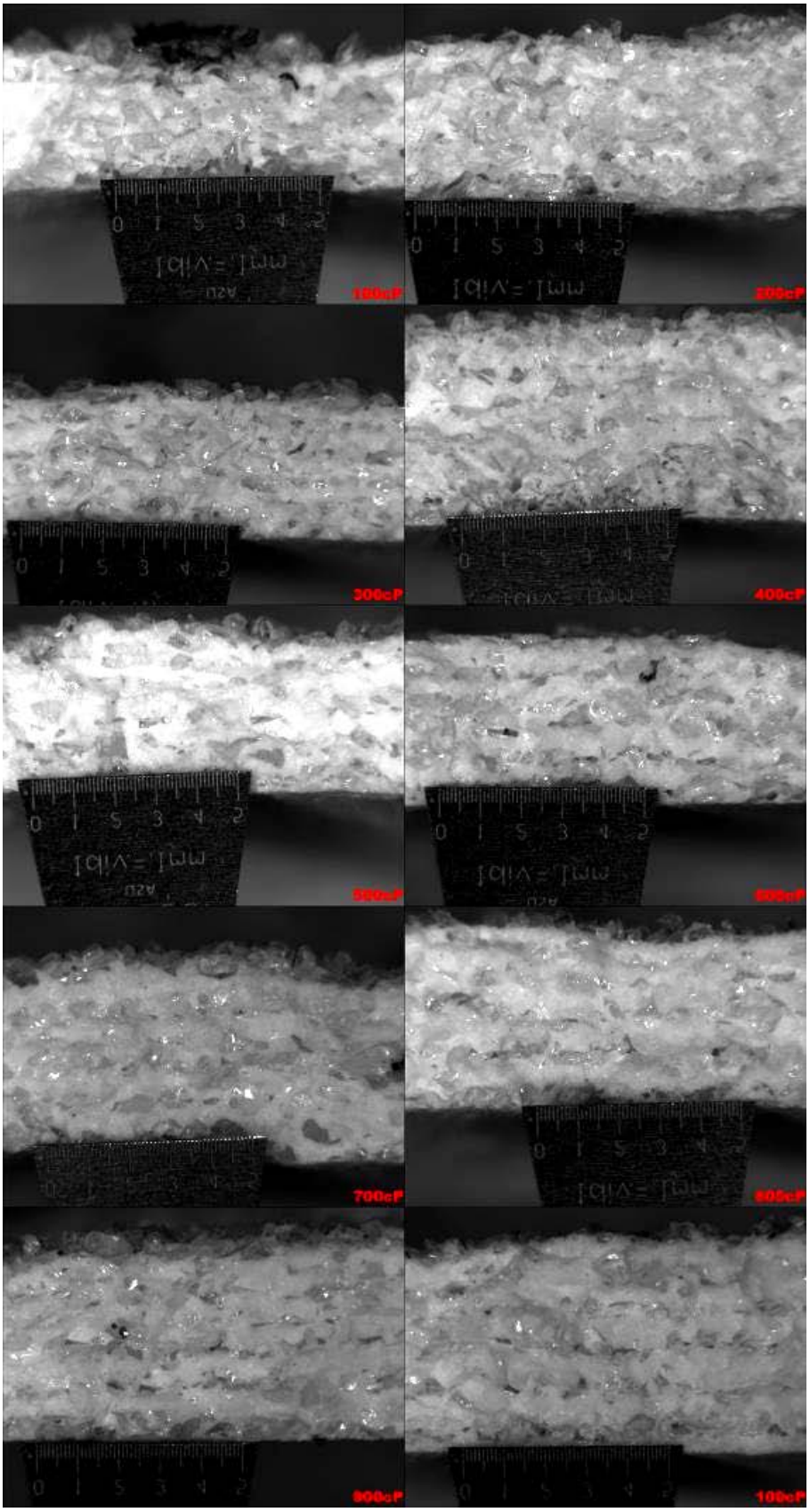

Figure 3.11 Cross-section views of samples created using different slurry viscosities

Between 100-300cP the stucco particles are aligned in a seemingly random pattern with minimum flour material between them. From 800-1000cP the stucco particles are aligned on planes matching the top of each coating layer giving a stripped appearance. As the viscosity of the slurry increased within this range, more flour material was found to be contained between each stucco layer. The remaining range of 400-700cP, shows slight characteristics of the other two structures. The increased thickness of the coating slurry left more material between the stucco particles, which increased the distance between particles in separate layers. This gave a slightly layered structure to the stucco, the position of the stucco along those layers was scattered and not along a single plane like the test samples from higher viscosity slurries.

3.4.1.2. Porosity and Density Observations. An Archimedes test was used to determine the apparent open porosity, apparent specific gravity, and bulk density of the mold samples, as shown in Figure 3.12. When comparing samples from different slurry viscosities, two regions in the plot can be noticed. When observing the trend in the bulk density and specific gravity plots as a function of slurry viscosity, a region of decreasing value is seen for samples below a critical level of 400cP, while the region of higher viscosity shows the values become essentially constant. Samples from slurries below 400cP showed higher bulk density as the fluidity of the slurry increased. The result for apparent open porosity within the mold sample's volume also shows the same effect, but appears to reach a constant value at a slightly higher slurry viscosity.

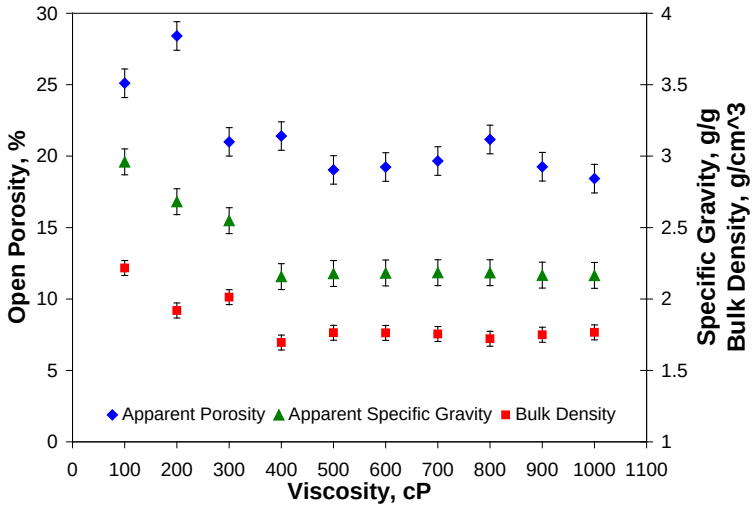

Figure 3.12 Changes in open porosity and particle packing as a function of slurry viscosity

This shift in open porosity and bulk density values matches well with the results of the visual inspection which determined a change in layer structure happened between slurry viscosities of 300cP and 400cP. Since the bulk density and apparent specific gravity both pertain to closed solid materials in the sample, open porosity levels have no effect on them. Since the stucco crystals and flour particles used in all samples were the same, this means that the voids between particles were decreasing in number and size. Since the bulk density was higher with more fluid slurries, it is concluded that the dried slurry in those samples was more tightly packed with less porosity inside.

The change in the apparent open porosity of the mold samples is a result of the changing slurry volume picked-up per coating. While the coating thickness was less than the diameter of the stucco particles, air would be present between stucco particles instead of only slurry. Those regions of air would continue through the molding process and finish as open porosity.

To determine the effect subsequent coatings have on the porosity, samples with different numbers of coatings were compared in Figure 3.13. When only two coatings were present, the volume of open porosity was much higher than that of the finished mold samples. With lower viscosity slurries this loss of open porosity was more significant during the first few coatings. This drop was a result of slurry filling in the air voids of previous coatings and taking the place of the previous open porosity. At four coatings and above the apparent open porosity appears to remain constant when lower viscosity slurries are used. For those coatings it is assumed that the volume of open porosity lost to slurry penetration is offset by the newly created open porosity of the newest layer.

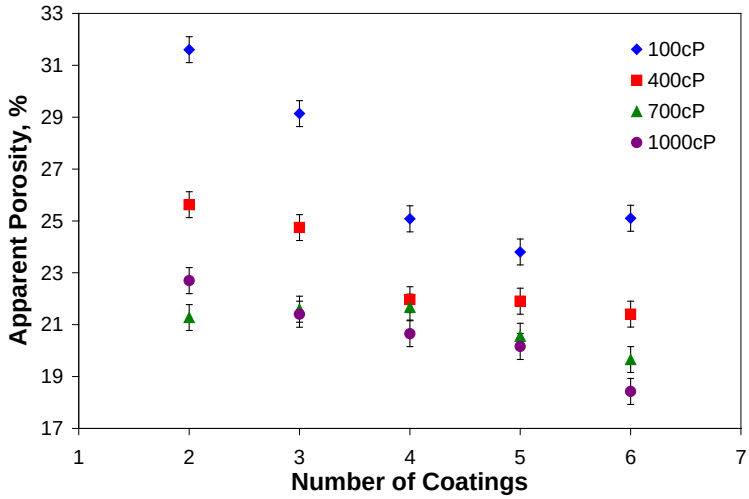

Figure 3.13 Apparent open porosity of the samples tended to drop as more coatings were applied

3.4.2. Permeability Testing. The difference in test sample thicknesses because of coating thickness and coating number required that the permeability data be

converted into a thickness independent form like volumetric air flux. When comparing the volumetric air flux through the test samples it was found that samples from the 100cP and 200cP slurries allowed for much higher gas expulsion rates, as shown in Figure 3.14. The remaining samples all displayed values ranging between 0.27 and 0.31mm/s, while the 200cP samples averaged 0.39mm/s and the 100cP samples averaged 0.45mm/s.

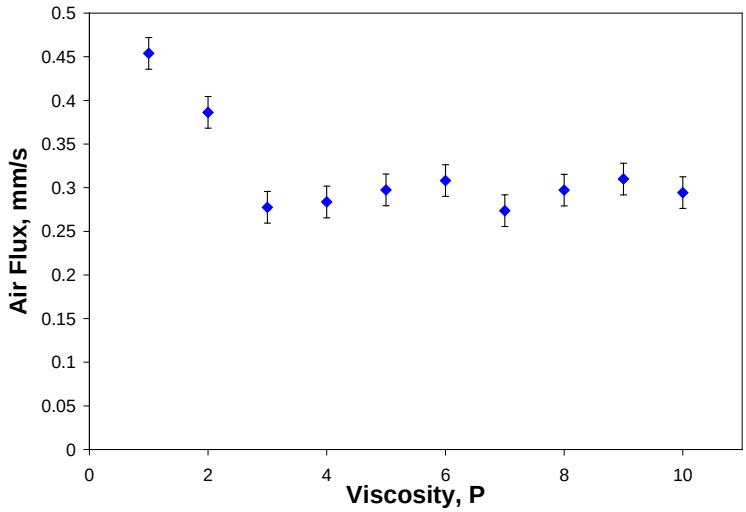

Figure 3.14 Rate of air flow through samples produced from a slurry of different viscosities

When comparing the volumetric air flux as a factor of coating numbers, a large drop in value was seen as the number of coatings increased as noticed in all plots of Figure 3.15. The volumetric air flux through only two layers was higher than the final value with a rate of 56mm/s being seen for the 100cP samples. The addition of the third coating blocked the majority of the air channels present in the previous layers dropping the volumetric air flux by 60-90% depending on the slurry used. The volumetric air flux

continued to decrease in an exponential fashion with more coatings until a common limit was reached. This limit is assumed to be the natural permeability of the dry slurry without the aid of structural porosity. The number of coatings required to reach this lower limit differed with slurry viscosity. The 1000cP samples reached a limit upon the third coating, while the 100cP samples were still just above the limit after the final sixth coat.

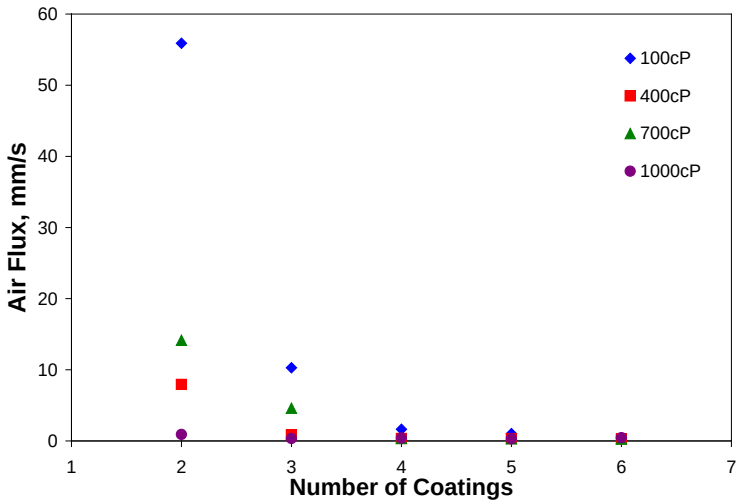

Figure 3.15 Change in air flow through samples as the number of coatings is changed

3.4.3. Strength Testing. When the test samples were cut to shape, it was found that many of the test samples using the very low viscosity slurry and few layers did not have sufficient strength to survive the normal cutting forces. When comparing the flexural strengths of the test samples with regard to their slurry's viscosity, it is seen that the higher viscosities produced stronger samples, as displayed in Figure 3.16. The adjusted fracture load of the samples from a lower viscosity slurry tended to be low with

a larger degree of scatter. Variations for these samples are assumed to be a random factor based on how closely the stucco particles were packed between layers instead of being caused by random defect locates within the samples.

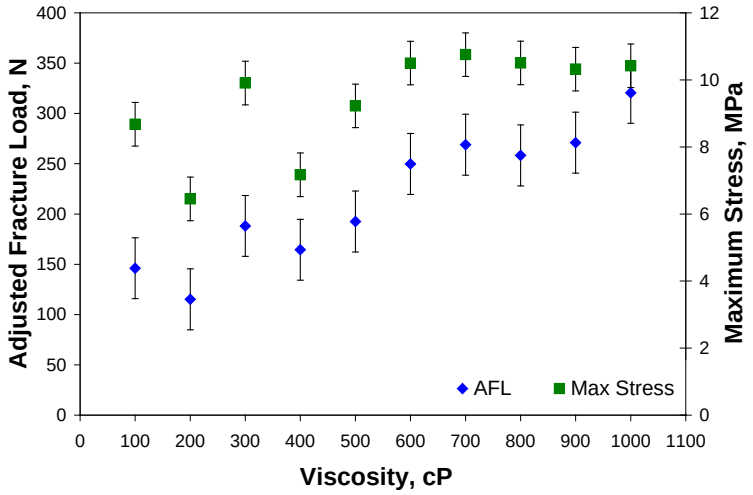

Figure 3.16 Maximum flexural loading and stress supported by test samples from slurries with different viscosities

Upon starting to develop a layered stucco pattern with the 400cP samples, the strength of the test samples gradually increased. Once the structure of the samples started to show a fully layered stucco separation at 700cP and higher, the flexural stress capacity of the test samples remained the same.

When examining the strength buildup of the test samples with different numbers of coatings, presented in Figure 3.17, the increase in strength appears to be nearly linear for all samples. Although the 700cP test samples initially are weaker than the 1000cP test samples, the two start to become close in value half way through the coating process.

At the other end of the test spectrum, the 100cP and 400cP test samples increase in load bearing strength at approximately the same rate. When looking at the linear regression equations for the samples it is found that the predicted value of a test sample with only one coating would have negative strength. While it is not possible for a test sample to have less than zero strength, it can be inferred from the frailty of the 100cP two coat samples that samples with only one coating would have near zero strength if making them as a continuously solid piece was possible.

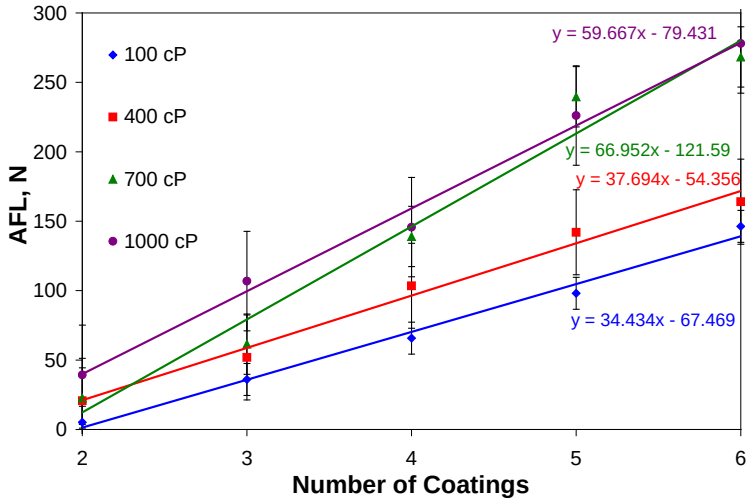

Figure 3.17 Increase in strength through additional coatings

3.5. ALTERING MOLD STRUCTURE USING SACRIFICIAL PARTICLES

When changing the mold structure by altering slurry viscosity, it was noticed that the permeability of the samples quickly lowered with the addition of more coatings. One of the reasons for this loss of air flow channels are the channels being filled in by new slurry during subsequent dip coatings. To prevent slurry from filling in and removing

possible air channels a method of creating porosity in a mold that was impervious to slurry flow had to be devised. To address this issue, graphite particles using a size distribution given in Table 3.6 were added to the slurry. The graphite particles would be embedded into the mold during dipping and upon firing the graphite would be removed leaving porosity. Graphite particles were ideal for this method since they were of a similar density to the slurry and would not chemically react with other materials.

Table 3.6 Particle Distribution of Graphite Additions

Sieve Analysis		
%+16mesh	(1180um)	0
%+20mesh	(850um)	2.33
%+60mesh	(250um)	81.4
%+80mesh	(180um)	9.73
%+100mesh	(150um)	4.2
%-100mesh	(150um)	2.35

For this test, the base one part binder to two parts flour slurry was mixed and then a set quantity of graphite particles was added to the mix based on the added weight of the other materials. Based on the previous test results, the slurry's dynamic viscosity during coatings was lowered to a range from 300-400cP. It should be noted that since the viscosity measured is a dynamic viscosity the presence of larger particles like the graphite would increase the reading. So, while the readings were set to the 300-400cP range, the dynamic viscosity of the slurry alone would have been even lower.

3.5.1. Graphite Generated Porosity. Test samples were cut in the green condition and an Archimedes test was performed before firing, as shown in Figure 3.18a.

The same samples were again tested, for Figure 3.18b, following firing and graphite removal to determine the change in porosity. It was found that the while the graphite lowered the apparent porosity of the green samples, they showed more open porosity following firing.

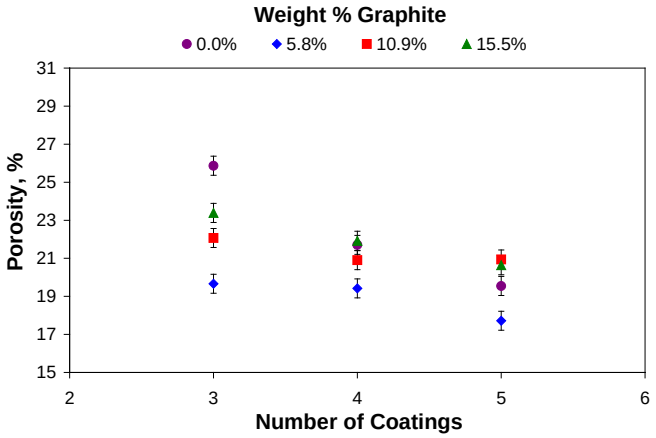

(a)

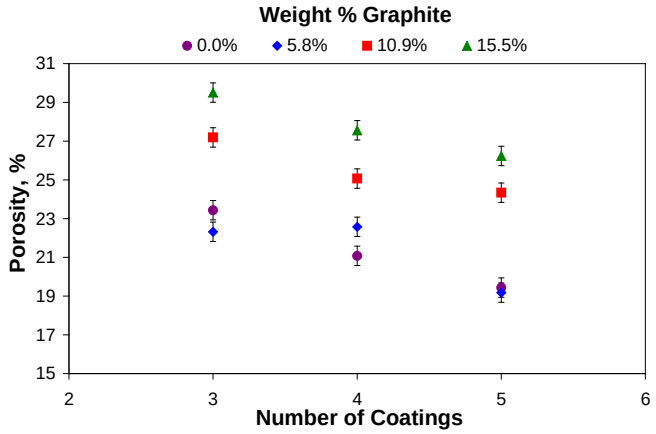

(b)

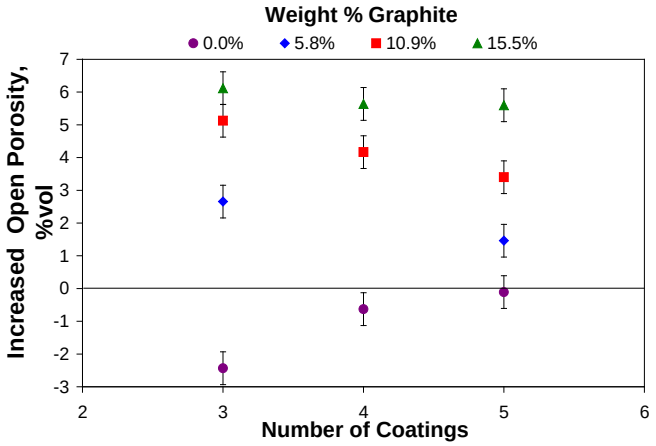

(c)

Figure 3.18 Open porosity values of samples with different percentages of graphite in their slurry (a) before firing, (b) after firing, and (c) the difference between them

When comparing the change in porosity before and after firing, using Figure 3.18c, the greatest increase was for the samples containing the highest concentration of graphite. The standard samples without graphite displayed a decrease in open porosity because of sintering. This means that the actual benefit of the graphite is not completely shown in the plot since sintering is not factored in the data points. The test samples with 15.5wt% graphite showed a uniform volume increase of open porosity following firings, regardless of the number of coatings. This means that the open porosity added in one layer was connected with the open porosity added in the neighboring layers. The other graphite concentrations tested showed decreasing graphite-generated porosity as more coatings were applied meaning that graphite particles in internal coating layers were being isolated and forming undesired closed porosity.

From monitoring the weight change of the test samples before and after firing, the quantity of graphite inside could be determined based on the weight lost. The calculated graphite volume in the unfired samples was compared with the increase in open porosity. This comparison shows the amount of the graphite which was in contact with other graphite or air voids and contributed to improving volumetric air flux after being burned out. The samples from the 15.5wt% graphite slurry had significantly more graphite pores being open (+40%) then those from the other slurries (~33%).

3.5.2. Permeability of Graphite Containing Slurry. The test samples with higher concentrations of graphite inside displayed the fastest rates of air flow through them, as presented in Figure 3.19. The volumetric air flux of the samples did decrease as more coatings were applied but the rate of decrease was not as steep as previously tested for slurries without graphite additions. The use of 15.5wt% graphite in the slurry

produced test samples that had a volumetric air flux of 0.97mm/s with three coatings but slowed to 0.43mm/s after five coatings were present. When compared to the volumetric air fluxes through the other test groups, the air rate through the five coating sample was near the same as for three coatings of the 5.8wt% graphite slurry.

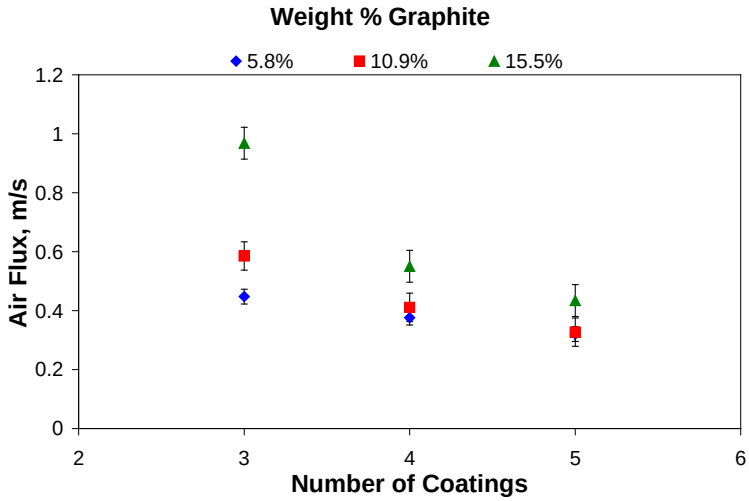

Figure 3.19 Air flow rate through samples containing graphite generated porosity

3.5.3. Strength Alterations from Graphite Additions. The flexural strength of the test molds were tested to determine if any adverse effects from increasing internal porosity were detectable. Contrary to initial assumptions, the addition of graphite into the slurry seemed to increase the load supporting ability of the samples, as is shown in Figure 3.20. For graphite concentrations at and below 10.9wt%, the resulting mold structure increased both strength and crack deflection. The test samples from the 15.5wt% graphite slurry are assumed to also contain these same benefits, but the larger

volume of pores counteracted those benefits giving those samples near the same loading strength as the original slurry.

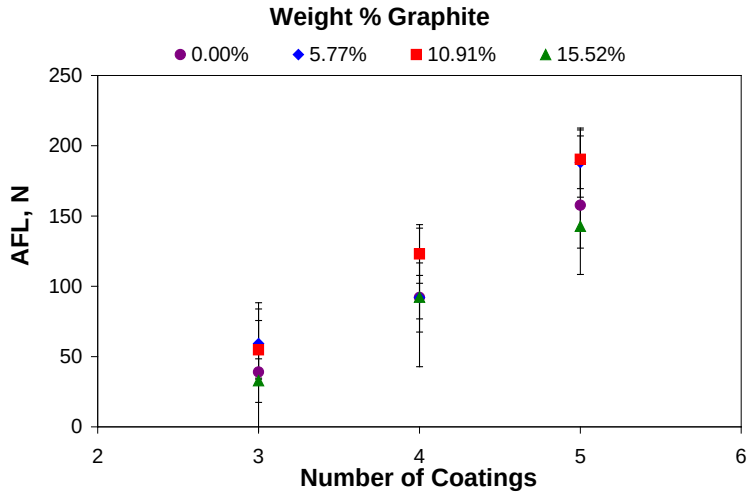

Figure 3.20 Maximum loading strengths of samples from slurries containing different concentrations of graphite particles

3.5.4. Simulation of Porous Coatings. At the same time as performing experimental testing on the samples, computer simulation models of the porous layers were created and analyzed. Two different types of models were investigated, a large volume with random pore placement and a narrow volume consisting of a single channel of pores. The large volume model was to determine the number of complete through channels based on the volume of pores and their size. The other model was used to analyze air flow through a single channel[21].

3.5.4.1. Random pore channel generation. For this three-dimensional Monte Carlo simulations were generated based on the physical parameters of the mold coatings

and graphite. The model was constructed to have the dimensions *H*x*L*x*L*, where the *L*x*L* faces were open to the air flow, and the *H*x*L* faces were assigned a boundary condition that prevented air flow from exiting the model from those sides. By setting the boundary conditions in that combination, it restricted the model to measuring volumetric air flux in only one direction, which matches with the assumptions commonly used when calculating permeability. The parameters *H* and *L* were set to values based on the mean pore diameter, *D*, with *L* being set to 100x*D* for all models and *H* ranging from 1.5 to 5 times *D* between different simulations.

The pores ranged in diameter between *D-dD* and *D+dD*, where *dD* was half the range of the graphite particle size distribution used in the laboratory experiments. The number of pores which were generated within each model was governed by an assigned fractional density, `r`. To randomly assign coordination for the graphite particles within the model, the Mersenne Twister algorithm[22] was used. Two restrictions were implemented on the placement of pore centers. One restriction was that the center of a pore could not be placed less than D-dD distance from another pore center to prevent overlapping. The other restriction was that a pore had to be a minimum distance of (D-dD)/2 from the outer edge. If a new set of coordinates violated either restriction that coordinate was omitted and a new one was generated.

A simulation routine was performed that generated a model and counted the number of complete pore channels connecting the opposing *L*x*L* faces of the model. This routine was run 1-10 million times for each permutation of volume height and pore fractional density tested. The results of all those runs are given in Figure 3.21. In the plot it is easily noticed that as the height of the model volume increased the number of

through channels decreased exponentially. This relationship matches with the results of the experimental testing which showed exponential drops in volumetric air flux with increasing numbers of coatings. As the fractional density of pores in the model increased, the number of through channels present also increased. This also matches with the experimental results where an increased concentration of graphite in the slurry resulted in greater volumetric air flux through the samples. At higher simulated pore concentrations, the relationship between number of channels and pore density slightly changes and it appears that a common value is shared by all models. This slight change can be accredited to the idea of the high porosity models nearing pore saturation where the number of through channels is independent of thickness.

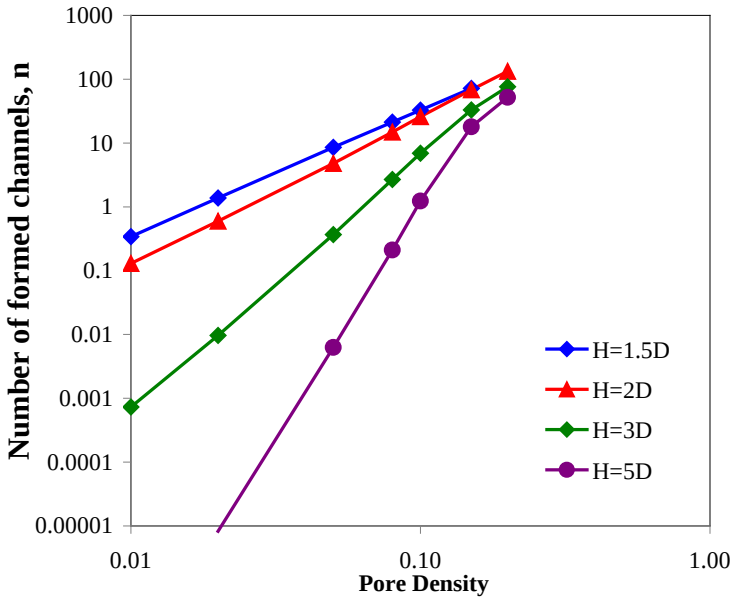

Figure 3.21 Number of predicted channels connecting opposing 100*D*x100*D* area faces

3.5.4.2. Single channel air flow. The air flow through individual channels was investigated by creating channel models consisting of three, four, and six pores connected to each other and forming a continuous path through the model. The pores were all given a diameter of 0.014in and the distance between the open surfaces of the volume was set to 0.039in. These values were chosen to match the average graphite particle size and the average coating layer thickness of the tested samples.

The pore channels were recreated in Fluent CFD so that dynamic air flow through the channel could be simulated. The pores were categorized as being hollow and capable of containing air flow. The surrounding media was defined as an impermeable solid, with a boundary condition between it and the pores preventing air flow into the solid. A pressure differential between the two ends of the channels was used to create flow through the channels.

A wide range of pressure differentials were simulated for each of the channel models. The superficial air velocity through the channels was directly recorded by the computer program and the Darcy permeability of the channels was back calculated based on the pressure differential used, the distance parallel to air flow, and the rate of air flow observed. The relationship between the superficial air velocity and the Darcy permeability for each model is shown in Figure 3.22. When the superficial air velocity remained below three centimeters per second, the viscous permeability of the channels remained uniform within the range of 50-60darcy. Superficial air velocities above three centimeters per second were observed through the simulation to create non-linear turbulent air flow within the pores. The turbulent air flow increased the inertial energy losses and created vortices within the spherical pores. For channels in which turbulent air

flow was generated, the Darcy permeability of the channels was approximately the same regardless of the number of pores making the channel.

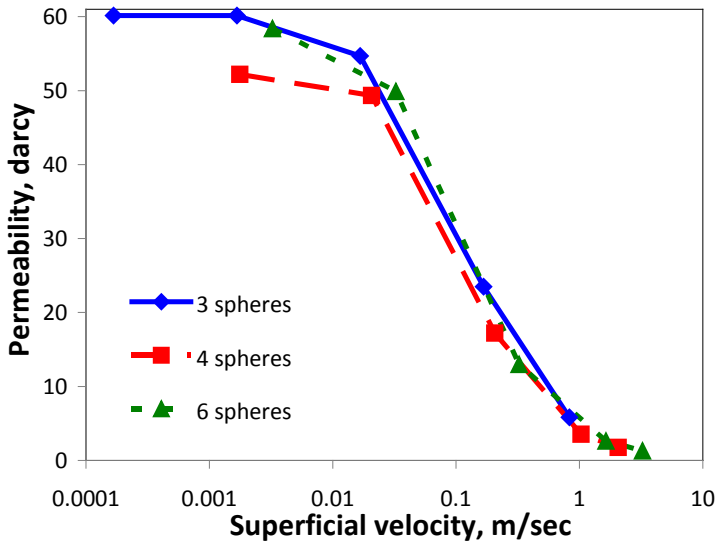

Figure 3.22 Predicted permeability of channels for different superficial air velocities

3.5.5. Comparison of Combined Simulation and Experimental Results.

The values of permeability through single channels were assigned to each through channel generated in the large volume models. This allowed for the prediction of specific permeability for each model. The results from combining the simulations in this manner are shown as curves in Figure 3.23 along with data points corresponding to the experimental results. The open porosity of only the channels in the test samples was calculated by taking the difference between the sample's open porosity and the open porosity of the corresponding sample without graphite additions. The experimental data points follow two different patterns; a low open porosity region of constant permeability

and a higher open porosity region were an increasing trend with permeability is present. This two part relationship matches that predicted by the simulation curves. The values during the initial constant specific permeability region are near zero as the simulation predicts. The values over four volume percent open porosity start to form a curve that is between the H=2D and H=3D curves. The position of the data curve matches what was predicted since the average coating layer thickness was equal to two to three graphite particle diameters.

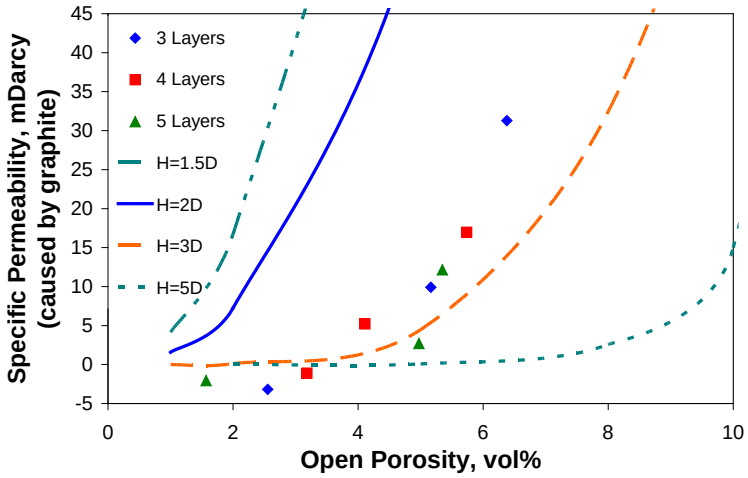

Figure 3.23 Experimental data points shown in relation to predicted trend curves

3.6. SECOND CASTING TRIAL

A final casting trial was designed to determine if the slurry alterations tested since the last casting trial would be sufficient to produce sound castings or not. The addition of 10.9wt% graphite into the slurry for all coatings was selected based on the improved

strength and permeability it provided over the base slurry. The coatings consisted of a prime, five backups, and a seal.

In addition, to trying to check castability using the new molds, the test was designed to determine effects the prime coat had on surface quality and permeability. To do this a mold was designed with two side filled horizontal plates (3.5x3x0.4in) and two bottom filled vertical plates (5x3x0.4in) all fed from the same sprue riser and is shown in Figure 3.24. Differing prime coat slurries were used for half the plates in each casting. A vertical and horizontal plate in each mold was coated with the 10.9wt% -200+800mesh graphite slurry selected. The other plates in the molds were either coated with slurry without graphite or slurry with 10.9wt% -100+200mesh graphite added. The pairings of prime coatings and pouring temperature into each mold is included in Table 3.7.

Table 3.7 Additions to Prime Coat Slurry and Pouring Temperature for Molds

Mold / Casting #	Graphite Type in Prime Coat			Superheat
	Large Particles	Small Particles	No Particles	
1	YES		YES	103°C
2	YES	YES		84°C
3	YES		YES	66°C

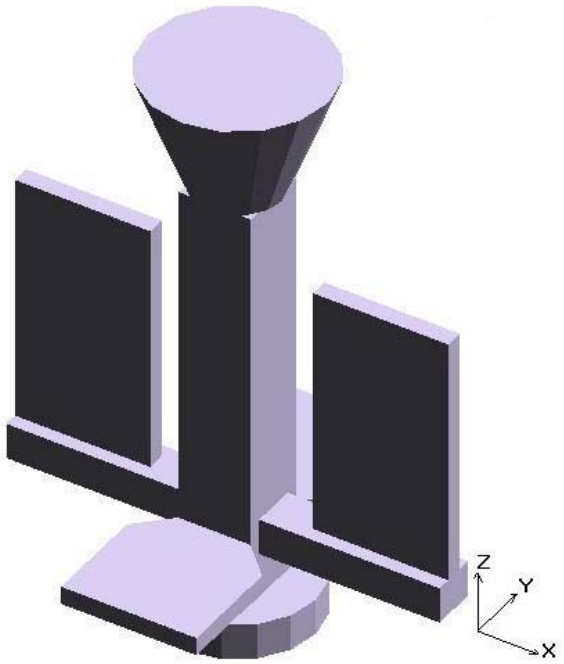

Figure 3.24 Model of the four plate mold used for casting trials

The molds were fired to 900C for four hours for pattern removal and then reheated to 800C prior to use. The steel alloy poured was HY130 modified to contain 5-5.5wt% nickel in the chemistry for improved fluidity. The steel was poured into the molds between 1600C and 1550C. The molds were filled in two to three seconds.

Table 3.8 Chemistry of March 2010 Heat

Element	C	Si	Mn	P	S	Cr	Mo	Ni	Al	Cu	Ti	V	Ca
Target	0.15	0.30	0.60	0.00	0.00	0.40	0.40	5.0	0.00	0.00	--	0.05	--
	0.18	0.60	0.90	0.01	0.01	0.70	0.65	5.5	0.07	0.05	--	0.10	--
Heat	0.13	0.31	0.52	0.00	0.01	0.64	0.45	4.1	0.06	0.06	0.00	0.07	0.00

3.6.1. Filling Height. The range of casting heights along the vertical plates, measured from the top of the runner to the top of the plate, in each casting were measured and plotted in Figure 3.25. It was observed that the plates from the graphite containing prime coats had a slightly higher casting height. In the mold containing graphite in all prime coats the horizontal plates filled to a greater height than any of the plates in the other molds.

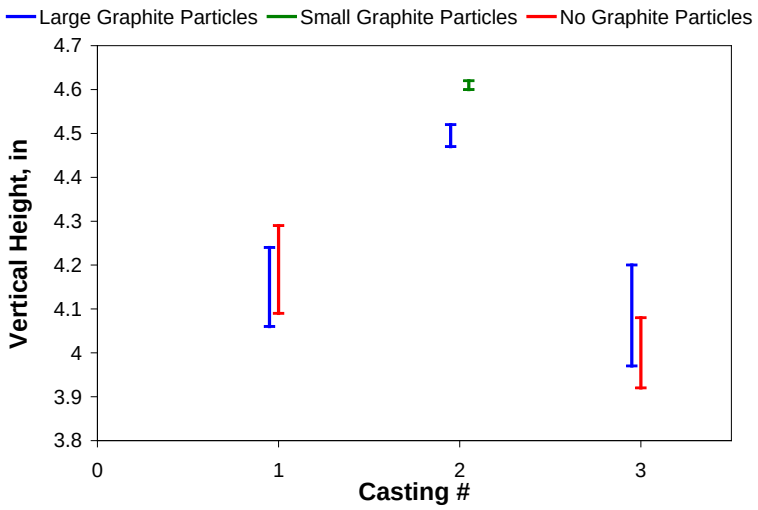

Figure 3.25 Range of fill heights from the gating up across the upper surface of the vertical plates

3.6.2. Surface Quality Transfer. The surfaces of the mold samples and the horizontally cast steel plates were scanned using a laser profiler. Four 8x8mm regions of each surface were selected randomly with the only criteria being that scans not overlap and no feature unique to a single small area be scanned. The scans measured surface height every 10um within the assigned regions for a total of 640,000 points per scan. For

comparisons between the mold and metal surface as well as between different metal plates, the range of heights (Sz) and root mean squared height (Sq) in each scanned area were calculated.

The use of large size graphite particles in the prime coat was apparent from the large range in Sz values of the mold, as seen in the plots for Figure 3.26. The mold surfaces which had contained large graphite particles showed the widest range of heights and also the most variation of that parameter over the whole surface. The other mold surfaces showed a narrower height range that was more consistent across the whole surface.

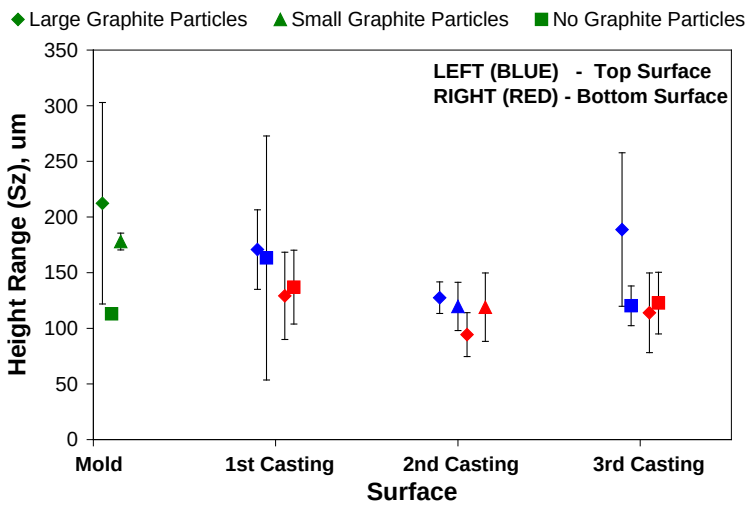

(a)

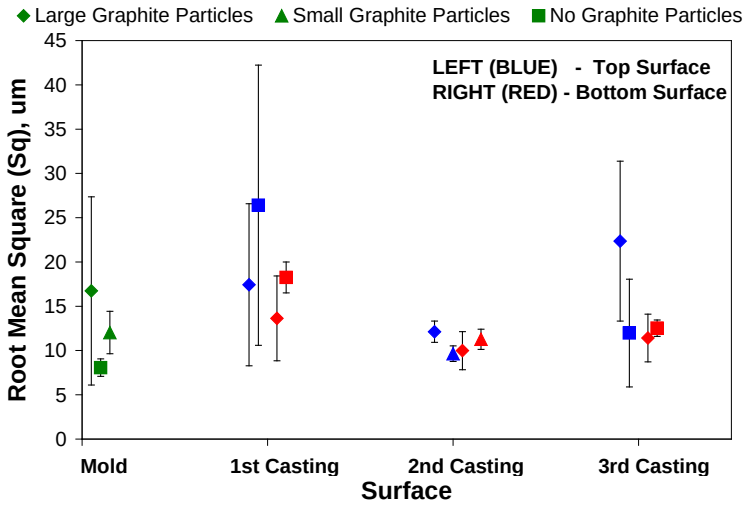

(b)

Figure 3.26 (a) Height range and (b) standard deviation of heights for scanned mold and as-cast steel plate surfaces

The top and bottom surfaces of the cast plates were analyzed separately since different factors affected each. Since gravity causes the molds to be filled from bottom to top, the bottom surface was more likely to be in contact with the mold surface. On the other hand, the top surface may not have contacted the upper mold surface depending on how well air was removed from the mold. This effect of air interference with the top

surface can be noted from the wider range of heights and higher roughness (Sq) of the top surfaces when compared with the matching bottom surface. In comparison with the matching bottom surfaces, those two parameters tended to be higher or the same for the top surface for all but casting #2 whose mold contained small graphite particles in the prime coat. The cause for the difference in that plate was because of adequate gas venting in that entire mold. As was seen for the fill height test, the upper surface was level without signs of gas interference. The reason that the bottom surface was slightly rougher is that gravity assisted the metal to penetrate into grooves and holes along the bottom.

The topography of the mold surface had only a slight transference onto the plate surfaces. The bead structure of the EPS which was transferred to the molds was only seen in rare locations along the bottom surfaces of the more permeable molds. In general, the height and roughness of the as-cast plate surfaces were higher than the molds' without graphite particles, but lower than the molds' when large graphite particles were used in the prime coat. This offset from both mold extremes shows that there is a limit to the fineness of details a cast surface can pickup from the mold. It also shows that there is also a limit to how much a casting can be affected by small air channels on the mold surface.

4. COMPARISON OF RESULTS AND CONCLUSIONS

4.1 CHANGES IN MECHANICAL PROPERTIES THROUGHOUT THE RESEARCH

Throughout all the experiments performed for this research, the strength and permeability of the molds were continually changing. The molds from the experiment that used different size distributions of stucco displayed a large range of load bearing capacities with little variation in volumetric air flux in comparison to the other experiments. The molds created from graphite containing slurry presented a wide range of volumetric air flux values with only slight changes in strength. The experiment that used different slurry viscosities showed a way to greatly improve one mechanical property at the expense of another.

The first molds were made with only fused silica flour, colloidal silica binder, and fused silica stucco using a moderate slurry viscosity of 700cP. Those molds could support an adjusted fracture load of 355N when -30+50 mesh stucco was applied for a mold sample with six coating layers, as shown under closer observation in Figure 4.1. Because of the high slurry coating thickness associated with the viscosity used in that test, the volumetric air flux through the samples was low for all samples with little difference based on testing variables.

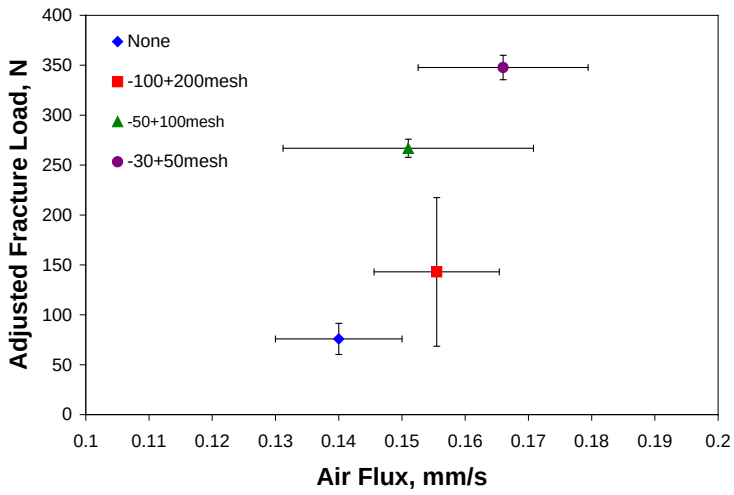

Figure 4.1 AFL and volumetric air flux correlation when varying stucco size

When the viscosity of the slurry started to be altered for the next test, the adjusted fracture load and volumetric air flux changed slightly, but some of that difference is because of those samples having one less coating layer. By changing the slurry viscosity, the coating thickness was altered and a range of macro-scale structures were formed in the molds. These changes in structure account for the changes in mechanical properties not related to the slight difference in the number of coatings.

The idea of classifying the mold structures into three categories, presented back in section 3.4, is presented again here based on the apparent grouping of the viscosity experiment's data points in Figure 4.2. The data points from the 100cP and 200cP slurries, which formed monolithic mold structures, averaged over 1.3 times more air flow then the other samples from that experiment, but both viscosity values produced molds which could not support an adjusted loading of 150N. The molds with a semi-layered structure, produced with slurry viscosities between 300cP and 500cP, had volumetric air

flux values of 0.27-0.30mm/s and adjusted fracture loads all between 150N and 200N. When higher slurry viscosities are used, and the mold structure becomes fully layered, the volumetric air flux remains the same as for a semi-layered structure but the adjusted fracture load significantly increases because of increasing coating thicknesses.

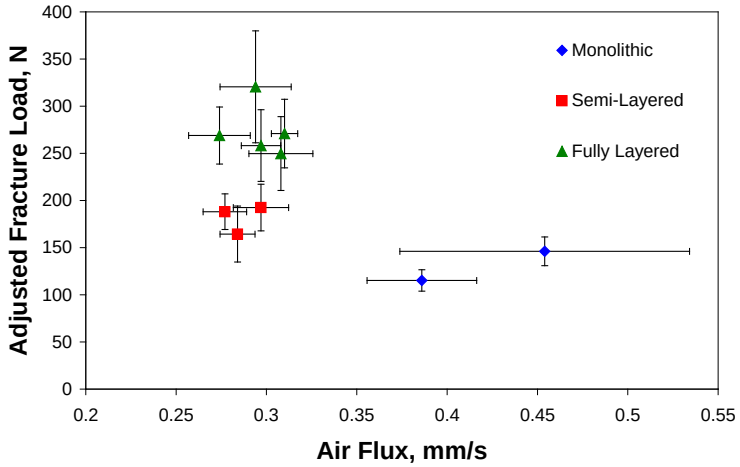

Figure 4.2 AFL and volumetric air flux correlation when varying slurry viscosity

When graphite particles were added to the slurry with 400cP viscosity, the load bearing capacity of the molds remained the same but increases in volumetric air flux were noticed. The adjusted fracture load for all the samples from the variable graphite experiment remained in the same 150-200N range as the previously tested samples with semi-layered structures. The volumetric air flux for the base samples without graphite remained the same as in the previous test, but the volumetric air flux showed a slight increase when graphite was added in concentrations below 11wt%. For the samples with

15.5wt% graphite particles added to their slurry, the volumetric air flux significantly increased over previous results by nearly 1.5 times the previous levels.

Another parameter investigated during the graphite varying experiment was the number of coatings making up the molds. When the volumetric air flux to adjusted fracture load relationship is shown for samples of three, four, and five coating layers, trends related to coatings are observed in Figure 4.3. When additional coatings are applied to the molds the volumetric air flux through the mold decreases and the load capacity increases. This trade appears to not be linear, but instead appears to follow a logarithmic curve. As the concentration of graphite particles in the slurry increased, the curve of the trend appears to broaden giving closer values of volumetric air flux with many coatings present and a wider difference in values earlier into the coating process.

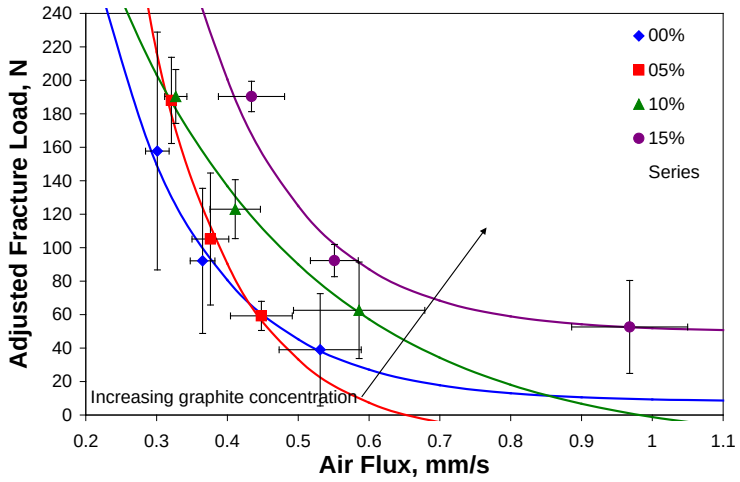

Figure 4.3 AFL and volumetric air flux relationship when varying graphite concentrations in slurry

4.2 RECOMMENDATIONS

The main objective of this research was to design a procedure for formulating investment casting molds and to determine alterations to the process to change mechanical mold properties. The addition of sacrificial particles, like graphite, in the slurry was shown to be a reliable method for increasing mold porosity and increasing air flow through the mold. The optimum ratio of graphite to flour to binder has not been fully explored in this experiment, so an ideal ratio can not be completely recommended. It was determined that between 10.9wt% and 15.5wt% graphite in a 2:1 flour to binder ratio the probability of pores aligning to form complete channels through the mold greatly increases. While the addition of more graphite into the slurry creates slightly weaker molds, the weakening is not significant when compared with the strength of a mold made from normal slurry without graphite at high viscosities.

The addition of graphite into the slurry at concentrations near 15wt% gives a significant increase to volumetric air flux without significantly lowering the mold's load bearing capacity. An additional method of improving volumetric air flux was to dilute the slurry making it more viscous. Lower viscosity decreased the coating thickness and resulted in a decreased media to stucco ratio.

On the other hand if the mold has problems supporting the pouring forces or internal pressures, then it is recommended to increase the thickness of the mold. This can easily be done by applying more coatings but will commonly decrease the air flow through the mold exponentially. Another method of strengthening the molds is to increase the slurry viscosity. Once a coating thickness that forms a fully layered structure

is reached the increased coating thickness from higher viscosities will carry over to the mold and increase the overall thickness.

With these general recommendations it should be possible to optimize currently used slurry to meet the physical requirements needed. Since the load bearing requirement vary based on pattern materials and their thermal expansion rates as well as pouring height into the mold a required minimum strength will vary between each foundry. Also, the minimum volumetric air flux for the mold is dependent on the pouring rate into the mold, the presence of open risers or vents, and the surface area of top risers. All these factors need to be considered when trying to optimize a molding process.

5. AREAS FOR FUTURE INTEREST

During the course of this research, many other topics of interest presented themselves, but were not pursued because of limitations on time or resources. Following are descriptions of areas for future investigations, why they are of importance, and how they would be tested.

5.1. DETERMINING THE MINIMUM PERMEABILITY OF A MOLD FOR COMPLETE CASTING.

The final casting trial of the research presented in this thesis started to address this topic, but would require many differing molds to be constructed and cast in. While the permeability of the final molds constructed was nearly sufficient to allow complete vertical mold filling, the actual permeability limit needed for complete filling was not determined. To address this topic, additional molds with differing air expulsion rates would be required. There are a few different methods to creating molds that expel air volume at different rates.

5.1.1. Varying Coating Thickness. The first method would be to vary the number of coating layers applied to the mold. It was found during the research that the volumetric air flux through the mold decreased as the thickness of the mold increased.

There are a few restrictions when using this method to vary volumetric air flux. The first restriction is that the change in volumetric air flux when applying different numbers of coatings is dependent on the concentration of large pores in the mold. If the concentration of large pores is below a certain level then the change in volumetric air flux between coatings may be too great for an accurate study.

Another restriction with this method is that differences in volumetric air flux are most significant when only a small number of coating layers are present. The problem with using molds with few coating layers is that the strength of the mold is not significantly increased yet. For those molds all the channels of large holes helping air flow could double as macro cracks leading to mold failure.

5.1.2. Varying Pore Concentration. A different method to form molds with different air flow rates is to change the open porosity of the mold by creating more large size pores. By using slurries with different concentrations of sacrificial fugitive, the mold's efficiency of removing air from the internal cavity can be varied in a controlled way.

The main drawback to this approach is that different slurry needs to be produced for each testing value. This method would require the most time of any method since the usual mold production time would be multiplied by the number of slurries required.

5.1.3. Varying Surface Area to Internal Volume Ratio. The final method to alter air expulsion rates from a mold is to change the pattern instead of the molding process. Since the volumetric air flux through the mold is related to the superficial air flow velocity and the internal surface of the mold in contact to the air by equation 5, presented above, the air expulsion rate can be altered by changing the surface area at the ends of the mold.

While this method has the benefit of only requiring a single slurry and coating procedure for all molds, it requires multiple patterns to be assembled that differ in surface area. For a comparison between molds, the areas first filled by metal would have to be the same for all patterns. Ideally the part of the pattern adjusted would be blind risers at

the end or top of the casting. The use of these locations are additionally required since the altered part of the mold can only affect air flow as long as it is not filled with metal.

Another restriction with this method is that it requires complete filling in the direction from the ingate to the altered area. If there are air pockets inside the mold not connected to the altered area, then air from those pockets will be expelled at the same rate for all molds. To prevent the separation of air into multiple pockets the geometry in the casting should not contain sharp corners and should be bottom filled.

5.2. CONCERNS REGARDING GREEN PERMEABILITY.

The use of graphite as a sacrificial additive to the mold slurry was found to increase mold permeability but does not produce that benefit in the green condition. Before the graphite is burned out of the mold during firing, the mold has low permeability like the initial molds testing in this research. This can present a problem during the pattern removal process that takes place before mold firing.

A low permeability green mold will not have the benefit of allowing liquid wax or foam vapors to flow into the mold to relieve stress from thermal pattern expansion. The removal of pattern material and the resulting stress relief will be dominantly affected by the opening of the sprue. This limitation on the removal of pattern material will generate higher pressure on the inside of the mold and can lead to cracking or bursting during that stage of the molding process. The only positive note is that before the removal of the graphite, the mold is less porous resulting in it having a higher strength then a mold with more porosity.

To deal with this issue, an alternate method of generating mold porosity may need to be determined that can be done without heating the mold. One option is to use particles that can be removed chemically instead of through burning. By replacing the graphite particles with a different material which can be dissolved in a chemical solution, increased porosity in the mold can be generated before pattern removal. Restriction on this option are that the sacrificial additives still need to be near the same density as the liquid slurry to stay in suspension and both the additive and the solvent need to be chemically inert with the mold materials. The solvent would not need to be chemically inert towards the pattern material, but should not cause increases in volume or leave solid residues within the mold.

5.3. VISCOSITY EFFECTS ON DIFFERENT PARTICLE SIZE DISTRIBUTIONS.

The main testing for this research dealt with only a single range of fused silica flour size and predominately only a single distribution of silica stucco particles sizes. The formation of either a monolithic or layered structure through the mold would still be dependent on slurry viscosity regardless of particles sizes, but the viscosities that form each structure would differ for other particle sizes. Since the mold will have a monolithic structure whenever the diameter of the stucco particles exceeds the coating thickness of the slurry, larger stucco particles will form monolithic mold structures with more viscous slurry then smaller stucco particles will.

Another area of possible concern is the effect of large particles, like the graphite proposed in this research, on rheological testing of the slurry. The presence of large particles can block slurry flow through small openings. This problem can prevent the use

of certain size Zahn cups and Ford cups commonly used in industrial facilities. This may lead to the need for taking dynamic viscosity measurements instead of measuring flow rates through an opening. When using graphite containing slurry, it was noticed that the dynamic viscosity of the slurry greatly increased with the addition of the large graphite particles. The increase to dynamic viscosity was mainly from the presence of large particles and not from the aqueous silica solution changing greatly. When diluting the slurry back to a lower dynamic viscosity it was observed that the aqueous portion of the slurry was far less viscous then previously. This viscosity decrease in the aqueous portion of the slurry may have created a more monolithic mold structure then originally planned since the graphite particles would be like stucco once in contact with the mold surfaces and no longer affect the aqueous slurry movement.

The large particles of graphite would also affect rheological measurements based on flow rate through an opening. The large particles would interrupt flow patterns increasing fluid turbulence and result in higher frictional energy losses. This slowing of flow would present a lower flow rate measurement of the slurry then the actual flow rate of the aqueous portion of the slurry.

In the experiment performed, the target slurry viscosity was originally targeted at a level based on molds without large particles in their slurry. While it was acceptable for initial study and variable comparison within the experiment, the mold structure formed from the aqueous silica portion of the slurry may not match that of the previous mold samples from 400cP slurry. To allow for more accurate comparison between experiments and to optimize the molding process further, the mold structure should be

observed when varying slurry viscosity after graphite particle additions. This experiment could be performed in the same way as the variable viscosity experiment presented in this research, but with the slurries produced for the variable graphite experiment.

APPENDIX

The physical properties for the materials used in the MAGMAsoft simulations are compiled here.

Properties for Silica Investment Molds:

Table A.1 Mold Specific Heat Capacity

Temperature [°C]	Cp [J/kgK]
50	600
100	700
150	750
200	800
225	1250
250	750
300	700
350	700
400	750
450	800
500	850
550	900
600	950
650	1000
700	1150
750	1300
800	1450
850	1600
900	1800
950	2000
1000	2250
1050	2300
1100	2400
1150	2400
1200	2400
1250	2500
1650	2500

Table A.2 Mold Permeability

Permeability [cm^3/min]	0.1540

Table A.3 Mold Thermal Conductivity

Temperature [°C]	Lambda [W/mK]
1	0.6821
300	1.3793
500	1.7925
900	2.5133
1100	3.1473
2000	3.1473

Table A.4 Mold Density

Temperature [°C]	Rho [kg/m^3]
0	1816
2000	1816

Properties of HY 130 Steel:

Table A.5 Steel Solidification Parameters

Solidus Temperature [°C]	1458
Liquidus Temperature [°C]	1494
Latent Heat [kJ/kg]	270.792
Feeding Effectivity [%]	30

Table A.6 Steel Fraction Solid

Temperature [°C]	fs
1458	1.00
1460	0.98
1470	0.84
1480	0.63
1490	0.26
1494	0.00

Table A.7 Steel Fluid Parameters

Flow Properties	
K0 [°C]	1467.00
K1 [°C/mbar]	0.00
K2 [°C/mbar^2]	0.00

Table A.8 Steel Liquid Viscosity

Temperature [°C]	Viscosity [m^2/s]
1	$1x10^{3}$
1458	$1x10^{3}$
1470	$1x10^{-2}$
1494	$7.43x10^{-7}$
1500	$5.75x10^{-7}$
1600	$4.37x10^{-7}$
2000	$4.37x10^{-7}$

Table A.9 Steel Thermal Conductivity

Temperature [°C]	Lambda [W/mK]
1	33.0
100	34.0
200	35.2
300	35.6
400	35.6
500	22.5
600	30.6
700	28.1
800	26.8
1000	28.5
1458	31.0
1487	30.0
2000	30.0

Table A.10 Steel Specific Heat Capacity

Temperature [°C]	Cp [J/kgK]
1	486.000
100	487.540
200	524.615
300	558.842
400	609.690
500	674.382
600	769.961
750	1080.000
800	640.105
1458	661.144
1487	750.000
2000	750.000

Table A.11 Steel Density

Temperature [°C]	Rho [kg/m^3]
1	7875
100	7850
200	7825
300	7800
400	7764
600	7714
800	7654
1000	7549
1200	7463
1300	7423
1400	7393
1458	7386
1460	7382
1470	7352
1480	7307
1490	7228
1494	7172
1600	7058
1700	6954
2000	6651

BIBLIOGRAPHY

1. G. X. Diamond, editor. Investment Casting Handbook 1980. Investment Casting Institute, pp 273

2. C.H. Matzek, Using Stucco More Effectively, Modern Casting, February 1988, pp50

3. M. Boccalini, E. Correa, Effect of Binder/Filler Ratio on Hot Strength and Hot Permeability of Investment Casting Ceramic Moulds, International Journal of Cast Metals Research, 1996, pp 133-137

4. B.A. Latella, L. Henkel, E.G. Mehrtens, Permeability and High Termperature Strength of Porous Mullite-Alumina Ceramics for Hot Gas Filtration, Journal of Material Science, vol 41, 2006, pp 423-430

5. C. Whitehouse, B. Dahlin, Effects of Wax Viscosity and Shell Permeability on Shell Cracking, Investment Casting Institute, 2008

6. B.S. Snyder, D.H. Scott, J.D. Snow, A New Combination Shell Strength and Permeability Test, Investment Casting Institute, v51, 2003, pp 11:1-26

7. M.J. Hendricks, M.J.P. Wang, R.A. Filbrun, D.K. Well, The Effect of Seal Dips on Ceramic Shell Properties and Performance, Investment Casting Institute, v50, 2002, pp 18:1-12

8. D. Austin, Percolation: Slipping through the Cracks, American Mathematics Society, Featured Column, Aug. 2008, archived at http://www.ams.org/samplings/feature-column/fcarc-percolation

9. K. Jancar, The Effect of Manufacturing Conditions on Some Properties of Molds, Precision Metal, Aug., 1969

10. J. Niles, The Effect of Slurry Viscosity and Stucco Size on Shell Properties, Investment Casting Institute, v48, 2000, pp 13:1-12

11. R.S. Doles, A New Approach to the Characterization and Optimization of Investment Casting Shell Systems, 9th World Conference on Investment Casting: San Francisco, California, USA, 1996, pp #8

12. M.J. Hendricks, Processing and Firing Influences on Ceramic Shell Materials, Foundry Trade Journal, June 1991

13. V.L. Richards, G. Connin, Four-Point Bend Testing to Characterize the Strength of Ceramic Mold Shells, Investment Casting Institute, v49, 2001, pp 13:1-10

14. V.L. Richards, S.A. Mascreen, P. Jackson, T. Hahn, Statistical Analysis of Three-Point and Four-Point Bend Testing for the Characterization of Ceramic Mold Shells, Investment Casting Institute, v51, 2003, pp 8:1-13

15. M.J. Hendricks, M.J.P. Wang, Ceramic Shell Green Strength – How is it Measured and What Does it Mean?, Investment Casting Institute, v47, 1999, pp 7:1-11

16. G. Barnes, P.A. Withney, The Mechanical Evaluation of Shell Moulds, Investment Casting Institute, v51, 2003, pp 9:1-9

17. P.C. Maity, J. Maity, Development of High Strength Ceramic Shell for Investment Casting, Indian Foundry Journal, v47, no7, 2001, pp 23-26

18. Y. Guzman, Certain Principles of Formation of Porous Ceramic Structures. Properties and Applications (A Review), Glass and Ceramics, v60, nos9-10, 2003, pp 280-283

19. P.H. Stauffer, Flux Flummoxed: A Proposal for Consistent Usage, Ground Water, v44, no2, 2006, pp 125-128

20. J. Chen, Personal Interview, August 20, 2008

21. S. Lekakh, Personal Interview, September 1, 2009

22. M. Matsumoto, T. Nishimura, Mersenne Twister: A 623-Dimensionally Equidistributed Uniform Pseudorandom Number Generator, ACM Trans. Modeling and Computer Simulations, vol. 8, 1998, pp 3-30

VITA

Darryl Michael Kline was born in Sturgis, Michigan on January 26, 1985. In May 2003 he graduated valedictorian from Tekonsha High School as well as received a certificate of completion from the Battle Creek Area Mathematics and Science Center. Three and a half years later, in November 2006 he received a B.S. degree in Mechanical Engineering from Rose-Hulman Institute of Technology, Terre Haute, Indiana. During the summers and the year after receiving his B.S. degree, he was employed as an engineering intern within the testing department of EATON Corporation's Automotive Proving Grounds located in Marshall, Michigan. In December 2010 he received a M.S. degree in Metallurgical Engineering from Missouri University of Science and Technology, Rolla, Missouri.

Darryl has been a member of American Foundry Society (AFS) since 2007 through which he has publish two technical articles in AFS Transactions as well as presented at Metalcasting Congress twice. In addition to authoring the technical articles, *Stucco Size Comparison and Simulated Pressure Loading of Investment Casting Shells* and *Improving Investment Casting Mold Permeability Using Graphite Particles*, he has also been co-author to two papers written by Dr. Simon Lekakh whom he frequently worked with.